Remarkable hole transport properties of Spiro[fluorene-9,9'-xanthene] derivatives containing natural amino acid substituents for perovskite photovoltaics

Hossein Askari,[a] Zahra Shariatinia,*,[a] Saeedeh Sarabadani-Tafreshi,[a,b] Nora H. de Leeuw[b,c]

[a]Department of Chemistry, Amirkabir University of Technology (Tehran Polytechnic),

P.O.Box:15875-4413, Tehran, Iran.

[b]School of Chemistry, University of Leeds, LS2 9JT Leeds, UK

[c]Department of Earth Sciences, Utrecht University, 3584 CB Utrecht, The Netherlands

*Corresponding author.
E-mail: shariati@aut.ac.ir

Abstract

Hole transporting material (HTM) highly affect efficiency and stability of perovskite solar cells (PSCs). Therefore, suitable HTMs should be designed to effectively extract and transfer holes in PSC devices. Herein, several HTMs were engineered composed of Spiro[fluorene-9,9'-xanthene] (SFX) core functionalized with natural twenty-one amino acids at the ortho, meta, and para positions of two SFX phenyl rings. Density functional theory (DFT) computations and Marcus hopping theory were performed to investigate various properties of these HTM derivatives. Highest occupied molecular orbitals (HOMOs) of all HTM samples, except for SFX-Asparagine, SFX-Glutamic acid, SFX-Glutamine, and SFX-Valine, were located between valence band of formamidinium lead iodide (FAPbI$_3$) perovskite and energy level of Ag cathode, which suggested these HTMs had efficient hole extraction and transport capabilities. Absorption spectra revealed that only SFX-Selenocysteine absorption occurred in visible region (λ_{abs}^{max}=800 nm), while absorption peaks all other molecules took place in ultraviolet (UV) area, similar to Spiro-OMeTAD. This was advantageous as it ensured that the HTMs had not any competition with perovskite material for sunlight absorption. Hole reorganization energies of all SFX-based materials, except for SFX-Serine and SFX-Histidine, were smaller than electron reorganization energies. Furthermore, hole mobility (μ_h) values of all HTMs were larger than (as big as 1000 times and higher) both of calculated (μ_h=5.65×10^{-3} cm^{2}V^{-1}s^{-1}) and experimental (μ_h=4.53×10^{-4} cm^{2}V^{-1}s^{-1}) values for Spiro-OMeTAD. This extraordinary result proved that all of the SFX-based molecules developed here had a high potential as alternative and more affordable HTMs to Spiro-OMeTAD.

Keywords: Perovskite solar cells; SFX core; Natural amino acids; Hole mobility; Exciton binding energy; DFT computations

1. Introduction

Sunlight can be used as a renewable energy resource for electricity generation. This is considered to be a green method as it avoids ecosystem pollution and weather alteration [1, 2]. Incident sunlight irradiation to the earth surface is the most plentiful (about 4×10^{24} Joules yearly) and benign energy resource [3]. Therefore, it can be exploited to fabricate photovoltaic devices [4, 5].

Organic-inorganic hybrid perovskites are attractive for many researchers as they have extensively been applied in PSCs in the past decades [6]. Due to their excellent photovoltaic properties and rapidly increasing performance, these materials are promising candidates for affordable solar cell technology and optoelectronic devices. Furthermore, in terms of power conversion efficiency (PCE), characteristics of PSCs such as cost efficiency, tenability, charge diffusion length, thermal and photochemical stability are significantly improved. Notably, FAPbI$_3$ is one of the most promising perovskite materials used in device fabrication [7].

In PSCs, solid HTMs are an important discovery replacing liquid electrolytes [8]. Utilizing HTMs for hole extraction from perovskite and its transportation towards electrode is imperative for most PSCs designs [9, 10]. A very famous HTM is 2,2′,7,7′-tetrakis (N,N-di-p-methoxyphenyl amine)-9,9′ spirobifluorene (Spiro-OMeTAD) that reveals low conductivity and hole mobility because of inherent trigonal pyramid structure, which causes long distances for its intermolecular interactions [11, 12]. Therefore, it must be doped with some chemicals doping such as lithium compounds to become more conductive and efficiently extract holes [13]. To overcome high cost and complexity of Spiro-OMeTAD synthesis, one of the alternatives is using SFX material due to its easy one-pot synthesis method [14]. Nonetheless, researchers were not interested to SFX since 1930 because its initial synthesis processes were not effective [15, 16].

An SFX compound containing one carboxylic acid and two phenol moieties was synthesized by condensing resorcinol and 9,10-diphenic-ketone-4-carboxylic acid using a $ZnCl_2$/HCl catalyst [17]. This SFX material has attracted much attention as eco-friendly and green organic semiconductor because of its easy production and binary conjugation of fluorene and xanthene moieties [18]. Green semiconductors need green synthesis precursors, environmentally friendly processes, and biodegradable or recyclable products [19, 20].

In the context of commercializing optical compounds, the main consistent fundamental parameters include processability, efficiency, price, and stability [21, 22]. SFX has become a powerful unit as it meets expected necessities because of crucial properties including accessibility, one-pot facile synthesis, and suitable efficiency [23]. Eco-friendly one-pot methods are significant in chemical industry to obtain fine chemicals [24]. In 2006, Xie and Huang prepared SFX and its several analogs using excess $MeSO_3H$ (85% yields) so that various halogenated phenols simply reacted with 9H-fluoren-9-one [18].

Herein, diverse SFX compounds containing 21 natural amino acids (Fig. 1) were devised for PSCs. For this purpose, amino acids as substitutions were first attached to the para, meta, and ortho positions of two phenyl rings onto the SFX molecule from the oxygen atom of COOH group to form C-O bonds. Then, DFT computations were carried out to optimize the SFX-based compounds and to find the most suitable HTMs with the best matched HOMO energy levels for hole transfer. It was found that the amino acids attached to the para positions had the most suitable energy levels. Also, to examine the effect of amino acids attached from the nitrogen atoms onto the SFX core, 21 HTM structures were drawn composed of C-N bonds at the para positions of two SFX phenyl rings. Interestingly, the HTMs containing amino acid substitutions that were attached from nitrogen atoms instead of oxygen atoms to the para positions demonstrated the most favorable

HOMO levels. In fact, their HOMO energies were the most satisfactory for application in PSCs based on SnO_2 electron transfer material (ETM), $FAPbI_3$ perovskite and Ag cathode. Hence, further DFT calculations were done on the SFX-amino acid derivatives with C-N bonds to explore their properties for application in PSC photovoltaics.

2. Computational approaches

Gaussian 03 package was used for DFT computational studies and structural optimization of twenty-one amino acid derivatives attached to the SFX core. It was revealed that among ωB97XD, B3LYP, CAM B3LYP, and MPW1PW91, approaches used together with 6–31G (d,p) basis set to calculate absorption spectrum of spiro[fluorenexanthene]-diol (SFX-OH), B3LYP/6-31G(d,p) illustrated an absorbance peak with the closest similarity to the experimental value [25]. As a result, B3LYP/6-31G(d,p) method was applied to minimize and attain absorption spectra of all HTM structures in both gaseous phase and in solvent (dichloromethane). Also, frontier molecular orbital (FMO), dipole moment, reorganization energy, and hole/electron mobility of all molecules were achieved by B3LYP/631G (d,p) method. The hole transport behaviors of the SFX derivatives were theoretically studied according to Marcus theory with hopping model [26].

Hole/electron reorganization energies (λ_h/λ_e) were obtained by Eqs. 1 and 2, where E_0^+ is energy of cationic structure from neutral structure, E_+ is energy of cationic molecule, E_+^0 indicates energy of neutral structure obtained from cation, and E_0 stands for energy of neutral structure. Similarly, E_0^- exhibits energy of anionic structure obtained from neutral form, E_- indicates energy of anionic form, and E_-^0 illustrates energy of neutral structure attained from anion [27, 28].

$$\lambda_h = [E_0^+ - E_+] + [E_+^0 - E_0] \qquad (1)$$

$$\lambda_e = [E_0^- - E_-] + [E_-^0 - E_0] \qquad (2)$$

Crystal structure data are essential to calculate transport integral, which includes two stages. Firstly, in Materials Studio package, geometry optimization was done using Dmol3 module. Here, twenty-one molecules were fully minimized by generalized gradient-correlated approximation (GGA) methodology based on the functional Perdew-Burke-Ernzerhof (PBE) and basis set DNP (double numeric polarized). As sum of ESP charges is not precisely 0.0 when using Dmol3 module due to truncation error, total charge was set at zero for optimized structures. Then, Dreiding force field was used to achieve crystalline structures by Polymorph prediction module. The Dreiding force field can well reproduce experimental results. To attain high accuracy and fine quality, ten important space groups including P212121, C2-C, P21, P-1, P21-C, C2, CC, PBCA, PBCN, and PNA21 were simulated.

3. Results and discussions

Herein, DFT computations have been done to explore optoelectronic, structural, and charge transport properties of varied SFX derivatives as HTMs of PSC devices. It is notable that the computational studies are able to predict the optoelectronic and structural properties of materials with a relatively high precision [29-31]. Also, there are lots of experimental researches on PSCs along with computational DFT methods performed on the HTMs used in the fabricated PSCs, which correctly predict various properties of materials used in solar cells and the device efficiencies [32-36]. Inspired by the satisfactory results achieved in similar literature, in this research, an attempt has been made to investigate and introduce suitable HTMs with favorable properties using DFT calculations and the validity of such computational studies has been confirmed in numerous researches published in literature. With the widespread usage and growing interest in organic semiconductors due to their versatile valuable properties for application in

various technologies like photovoltaics, thin field transistors, light emitting diodes, and other optoelectronic devices, their ionization potentials (IPs), electron affinities (EAs), and frontier molecular orbital energies should be accurately determined. Precise prediction of IPs/EAs helps in determining various properties like exciton binding energies and electron/hole injections, which play a crucial role in determining efficiencies of these devices. Besides, accurate calculation of HOMO/LUMO energy levels helps in selection of suitable electrodes for solar cells. Hence, a reliable theoretical methodology, which accurately predicts the above mentioned properties is required to design and develop the devices of higher efficiencies. DFT methods are widely popular and are regularly used to predict these properties. DFT provides a cost-effective computational method for calculating optoelectronic properties of relatively large molecular systems. In addition, widely-used DFT methods have been shown to systematically estimate optical, electrical, and structural properties.

Here, a general roadmap is presented using DFT method to study electronic structures and hole transport properties of materials for PSCs. Based on this method, a thorough analysis is done and one can decide if a molecule can be a suitable hole transport material or not. In fact, this can be regarded as a universally applicable guidance offered for future experimental or design endeavors. A favorable HTM should display the following properties to be used as an excellent material in PSC fabrication.

(1) A HOMO level energy between the valence band level of perovskite and Fermi level of cathode (Ag, Au, and so on). (2) A LUMO level that is higher than the conduction band level of perovskite to avoid back-transfer of electrons towards cathode electrode. (3) Lower electronegativity (χ) and electrophilicity index (ω) which exhibit low electron withdrawing property. (4) Smaller IP and EA. (5) Higher chemical potential (μ) and chemical hardness (η),

7

which confirm a higher stability. (6) Higher solubility, (7) More negative binding energy. (8) Lower exciton binding energy (E_b). (9) Higher LHE. (10) Higher hole mobility, lower reorganization energy, higher hole/electron transfer integral, and higher charge transfer rate. (11) Higher V_{OC}, FF, J_{SC}, and PCE values.

3.1. Optimization of geometries

It is well known that geometrical conformations can highly affect electronic and optical characteristics of molecules. Here, amino acid compounds have been substituted onto the SFX core in order to explore the best position of the desired substitutions by comparing the results obtained for the structures substituted at the ortho, meta, para positions. It was found that the para-substituted HTMs could more effectively transport holes from the $FAPbI_3$ towards the Ag cathode. Therefore, the influence of SFX binding to 21 natural amino acids from their nitrogen atoms, was additionally explored. As their HOMO energies displayed the most matching with the energy levels of materials used in fabrication of PSCs based on SnO_2 electron transfer material (ETM), $FAPbI_3$ perovskite and Ag cathode, additional DFT computations were conducted on the SFX-amino acid HTMs containing C-N bonds to unravel their characteristics. The optimized geometries of all designed HTMs with SFX attached to 21 natural amino acids by C-N bonds are demonstrated in Fig. 2.

3.2. Frontier molecular orbitals (FMOs)

Analyzing HOMO and lowest unoccupied molecular orbital (LUMO) energies helps to examine optoelectronic features and suggests transfer pathways for charges in molecules. Consequently, one can predict PSC efficiency based on the HOMO and LUMO energies. This is

8

because FMOs afford information regarding transmission of charge carriers within a material. Appropriate HOMO and LUMO energies lead are advantageous to improve the hole transfer features of HTMs.

FMOs describes the charge density distributions over a molecule. Fig. 3 illuminates HOMO and LUMO orbitals for SFX-based HTMs. Negative and positive charges are displayed with red and green colors, respectively. In most HTMs, HOMO orbitals are delocalized on the substituted amino acid groups but in some cases, they are spread specifically on terminal atoms of amino acid moieties. The HOMO orbitals of four structures including SFX-Asparagine, SFX-Glutamic acid, SFX-Glutamine, SFX-Lysine, and SFX-Valine are distributed over the three six-membered rings of SFX core. Almost in all samples, the LUMO orbitals are mainly localized onto the central SFX core. Besides, in some samples, HOMO orbitals are more dispersed on the molecules. This result may suggest that there is a more efficient interaction between the molecule's HOMO and the perovskite, leading to an enhanced hole transport ability of HTM compared to electron transportation.

Notably, FMOs are normally employed to illustrate charge transport properties of semiconductor materials because more delocalized FMOs can promote faster charge transport by reducing nuclear reorganization energy and increasing electronic coupling between adjacent molecules. The distribution of HOMO orbitals can influence hole mobility of investigated HTMs. When HOMO is widely spread over the molecule, there is a greater probability for more facilitated and effective generation and mobility of holes because there are more available sites to create/transport these mobile positive charges. Similarly, it has been shown that the delocalized HOMOs and the quasi-planar molecular architecture were beneficial for the electronic coupling

9

between adjacent molecules, which improved the hole transport capability foe the studied HTMs [37].

In order to find the most effective HTMs for PSCs with an architecture of FTO, SnO_2 ETM, $FAPbI_3$ perovskite, HTM, and Ag cathode, HOMO energies of SFX-based HTMs must be between valence band (VB) of $FAPbI_3$ (-5.74 eV) [38] and Ag energy level (-4.7 eV) [39]. In the PSCs, upon $FAPbI_3$ excitation by solar light, electron and hole production occurs. Light generated electron is injected to conduction band (CB) of SnO_2 and transported by SnO_2 to be received by conductive FTO glass. On the other hand, hole in VB of $FAPbI_3$ is transferred towards HOMO level of HTM. Accordingly, HOMO of HTM must be upper than VB of perovskite but lower than silver energy level. Also, LUMO of the HTM should be as high as possible with respect to the perovskite CB, because this higher energy level prevents electron back transport from $FAPbI_3$ toward HTM, thus declining electron-hole recombination [40].

It is noteworthy that in this work, Ag is used as the counter electrode instead of Au due to the following reasons. To commercialize perovskite solar cells (PSCs), it is important to substitute alternative electrodes by Au to decrease the unit cost. Also, Ag (silver) is commonly used as a cathode material in perovskite solar cells due to its high conductivity and stability. Here are a few reasons why Ag is preferred: **(1) Cost:** Ag is significantly cheaper than Au, making it more economically viable for large-scale production of perovskite solar cells. The lower cost of Ag can help reduce the overall production cost of the cells, making them more affordable and accessible. **(2) Optical properties:** Ag has excellent light absorption and scattering properties, which are important for efficient light absorption in PSCs. It has a high extinction coefficient and can effectively trap and confine light within the active layer, improving the overall device performance. **(3) Stability:** Silver is considered to be chemically stable, meaning it does not

readily react with other materials in PSC such as perovskite layer or electrolyte. Stability contributes to the long-term performance and durability of the device. For example, in PSCs fabricated with $MAPbI_3$ perovskite, the Au electrode can cause serious solar cell degradation due to Au diffusion into $MAPbI_3$ that results in strong non-radiative recombination. **(4) Reflectivity:** Silver has a good reflectivity property, which means it can enhance light trapping and absorption within PSC, thereby boosting the device performance.

The HOMO and LUMO energies of molecules optimized in gas phase containing 21 natural amino acids attached from oxygen atom of COOH group to ortho, meta, or para locations of two aromatic rings on SFX core are given in Tables S1-S3. Considering the HOMO levels of three series of HTMs, it is found that more number of materials composed of amino acids at the para positions of phenyl rings are suitable as hole transfer compounds compared to the samples containing amino acids at ortho or meta positions. Therefore, the para-substituted SFX samples were chosen as the most favorable HTMs. In next step, all of 21 amino acids were attached from nitrogen atom of NH group to the para positions of phenyl rings and it is obvious from the data in Table 1 that more number of these materials meet the criterion required for the satisfactory HTM compared to their counterparts attached from oxygen groups of COOH moieties to the SFX core. Thus, all DFT computations have been conducted on the HTMs with C-N bonds.

Table 1 presents HOMO, LUMO, and E_g values for HTMs containing natural amino acid substituents attached to para positions of aromatic rings of SFX core via nitrogen atom of NH group in dichloromethane solvent. Furthermore, Fig. 4 exhibits the energy levels of FTO, SnO_2, perovskite $FAPbI_3$, SFX-based HTMs, and Ag cathode. It is observed that except for four samples including SFX-Asparagine, SFX-Glutamic acid, SFX-Glutamine, and SFX-Valine, all of

remaining 17 materials are desirable HTMs for PSCs based on SnO_2 ETM, $FAPbI_3$ perovskite, and Ag cathode. Hence, further calculations are carried out on these samples.

The VB energy of $FAPBI_3$ is -5.74 eV and the E_{HOMO} of four SFX-Asparagine, SFX-Glutamic acid, SFX-Glutamine, and SFX-Valine derivatives are deeper than this level, approving they cannot transfer holes from perovskite towards the Ag cathode. Based on the formula $VB(FAPBI_3)–E_{HOMO}$, the energy barriers for hole transport in these materials are estimated. the HOMO energies of SFX-Asparagine, SFX-Glutamic acid, SFX-Glutamine, and SFX-Valine are equal to -5.747, -5.854, -5.851, and -3.817 eV (Table 1) and their hole transfer barriers are 0.007, 0.114, 0.111, and -1.923 eV, respectively.

The CB energy of $FAPBI_3$ is -4.27 eV and the E_{LUMO} of all SFX-based materials except for the SFX-Selenocysteine (-4.98 eV) are upper than this level, confirming they cannot transport electrons from perovskite to the SnO_2 ETM. To estimate the energy barrier for electron transport, the formula $E_{LUMO}–CB(FAPBI_3)$ can be used. As the LUMO levels of SFX-Serine and SFX-Lysine are the highest among all samples and located at -0.861 and -0.862 eV (Table 1), they indicate show the highest energy barriers of investigated SFX-based HTMs for electron transportation. Electron injecting energy barriers for SFX-Serine and SFX-Lysine are measured to be 3.409 and 3.408 eV.

The binding energy ($E_{binding}$) of all samples are provided in Table 1, which display they vary from -6590.435 kcal/mol (for SFX-Selenocysteine) to -11030.720 kcal/mol (for SFX-Tryptophan). The large negative $E_{binding}$ values of all HTMs verify that they have a highly stability.

3.3. Dipole moment and surface potentials

The dipole moments of HTMs estimate their solubility within solvent as there is a linear relationship between dipole moment and solubility. Data in in Table 1 reveal that the highest dipole

moment values of 8.516, 8.388, and 8.167 Debye are measured for SFX-Histidine, SFX-Valine, and SFX-Glutamine, demonstrating their high solubility in dichloromethane solvent. The lowest dipole moment values of 1.806 and 2.065 Debye are obtained for SFX-Cysteine and SFX-Arginine, exhibiting they have the least solubility in dichloromethane solution.

It is known that the most essential requirement of HTMs is suitable energy levels of HOMO and LUMO orbitals to match those of the perovskite layer. Also, efficient HTMs require additional features such as high solubility and film-forming property, which are beneficial for the device fabrication by spin-coating method. In fact, high HTM solubility results in optimization of molecular packing, film morphology/thickness, and effective interface contact with adjacent perovskite and cathode layers. Higher solubility enables a wider concentration range of HTM is used and deposited over the perovskite layer, which leads to optimum optoelectronic performance whereas lower solubility of HTM limits its use for PSCs due to reasons including **(1) processing challenges:** Low solubility often leads to difficulties in preparing uniform and smooth thin films during the fabrication of solar cells. This can result in poor coverage and uneven distribution of HTM, affecting overall device performance. **(2) Film morphology:** the solubility of a material is closely related to its ability to form a well-defined film. Indeed, low solubility of molecules might result in aggregated or poorly dispersed structures in their films, leading to increased charge recombination but decreased charge mobility.

Electrostatic surface potential (ESP) maps of all SFX-based HTM derivatives calculated in dichloromethane are presented in Fig. 5. It is found out that the spatial orientations of molecules can greatly affect the negative/positive charge dispersion on samples. In fact, molecules indicating more asymmetric charge distributions possess bigger dipole moments while more symmetrical charge spread over a molecule leads to a smaller dipole moment. Fig. S2 illustrates the contour

maps of SFX-based HTMs. Similar to the ESP maps, molecules with larger dipole moments exhibit a more asymmetric dispersion of positive and negative charges and vice versa. The contour maps are well consistent with the ESPs of SFX-based HTMs.

3.4. Quantum chemical descriptors

Quantum chemical descriptors are provided to analyze reactivity and stability of SFX-based materials. Table 2 displays the calculated descriptors for all samples. The chemical potential (μ) of a molecule describes its ability to donate electrons and can be calculated by Eq. (3) [41].

$$\mu = 1/2 \ [(E_{HOMO} + E_{LUMO})] \qquad (3)$$

The μ values of SFX-based materials change from -3.048 eV (for SFX-Leucine and SFX-Glycine) to -5.204 eV (for SFX-Selenocysteine). Consequently, all molecules are found to have higher negative chemical potential values than standard HTMs such as X65 with μ=-2.46 eV [25] and Spiro-OMeTAD (μ=-2.719 eV), demonstrating the SFX-based molecules are very stable.

Chemical hardness (η) and chemical softness (S) are determined via the Eqs. (4) and (5), respectively. Hardness is resistance of molecule against any changes of electron number that exhibits PSC stability, confirming a highly stable HTM can control device stability [42]. When HTM shows a larger η, it is a harder and more stable molecule [43]. The η values of SFX-based samples (except for SFX-Selenocysteine with η=0.226 eV) are in the range of 2.009 (for SFX-Methionine) to 2.353 eV (for SFX-Proline), which indicate the investigated molecules have very similar η values and thus comparable stabilities (except for SFX-Selenocysteine with the least stability).

$$\eta = 1/2 \ (E_{LUMO} - E_{HOMO}) \qquad (4)$$

$$S = 1/\eta \qquad (5)$$

The higher S value for a molecule suggests that it can effectively donate electrons and has a higher reactivity with its adjacent species. Comparing the chemical softness values exhibits that SFX-Selenocysteine with S=4.4170 eV has the highest softness, which is very different from other samples. For other HTMs, the S values are almost close to each other and change from 0.4250 eV (for SFX-Proline) to 0.4979 eV (for SFX-Methionine). These results validate that all of the studied molecules (except for SFX-Selenocysteine) have extremely low softness but SFX-Selenocysteine is the softest molecule along with the lowest band gap (0.453 eV) and highest chemical reactivity. It is notable that the stability of the SFX-based molecules is higher compared to that of famous HTM Spiro-OMeTAD (η=1.782 eV, S=0.561 eV).

Electronegativity (χ) and electrophilicity index (ω) are obtained by Eqs. (6) and (7), respectively, and both of them describe electron withdrawing property for a molecule. The χ and ω parameters vary in ranges of 3.048-5.204 eV and 3.065-13.350 eV, respectively, which verify they have remarkable electron attracting abilities. It should be noted that except for SFX-Selenocysteine with unusual properties among all HTMs, the uppermost χ and ω parameters are measured for SFX-Arginine but the lowest χ and ω are attained for both SFX-Glycine and SFX-Leucine.

Comparing the χ values of all samples indicates that the two HTMs including SFX-Leucine and SFX-Glycine have the lowest χ=3.048 eV. Also, except for SFX-Selenocysteine with unusual properties, the smallest ω values of 9.724 and 10.021 eV are measured for SFX-Leucine and SFX-Glycine, respectively. Therefore, considering the χ and ω values, these two samples are preferred over other molecules.

$$\chi = -1/2\ [(E_{HOMO} + E_{LUMO})] \tag{6}$$

$$\omega = 1/2\ [\mu^2/(\eta)] \tag{7}$$

Charge transfer properties of SFX-based molecules can be calculated using Eq. (8) as another crucial factor. Results in Table 2 show that charge transfer capability of all samples are greater compared to a HTM like X65 [25]. Furthermore, their charge transfer values are comparable to ΔN_{max}=1.526 calculated for Spiro-OMeTAD. Therefore, these SFX-based compounds can be applied as elite HTMs of PSCs. Except for SFX-Selenocysteine with unusually large ΔN_{max}=22.984, the smallest ΔN_{max}=1.376 belongs to SFX-Lysine whereas the biggest ΔN_{max}= 1.684 is attained for SFX-Arginine.

$$\Delta N_{max} = -\mu/\eta \tag{8}$$

3.5. Ionization potentials and electron affinity

Ionization potentials (IPs) and electron affinity (EA) are favorable descriptors for elucidation of charge transfer by HTMs. The IP and EA can be obtained using Eqs. (9) and (10), respectively, which calculate energies necessary to inject hole and electron [44]. In these formula, E_0, E^-, and E^+ signify neutral, anionic, and cationic molecules, respectively.

$$IP=E^+-E_0 \tag{9}$$

$$EA=E_0-E^- \tag{10}$$

A smaller IP indicates that the sample is a more suitable HTM whereas a larger EA>3 will result in a superior ETM [18]. Therefore, an ideal HTM should indicate the lowest EA and IP parameters. All IP and EA values in Table 3 illustrate that SFX-Selenocysteine has the lowest IP=5.124 eV but the biggest EA=15.043 eV. Hence, this molecule cannot be chosen as a suitable HTM because of it large EA value. Notably, the smallest EA values of 1.035 and 1.067 eV belong to SFX-Glycine and SFX-Alanine; also, it is seen that their IP values of 5.245 and 5.275 eV are

not very large among those of other samples. Thus, it may be found that these two sample can be favorable HTMs based on the IP and EA parameters.

3.6. Optical properties

Optical properties of HTMs can be estimated by their light harvesting efficiency (LHE) as a measure of sunlight photons absorption that is calculated by Eq. (11). A greater f_{abs}^{max} results in a superior LHE [45]. It is known that a HTM with a higher LHE more contributes in current generation by the PSC device [46].

$$LHE=1-10^{-f_{max}^{abs}} \quad (11)$$

Absorbance oscillation strength (f^{max}_{abs}), and LHE for investigated HTMs are presented in Table 3. The highest LHEs of SFX-Cysteine (0.927) and SFX-Alanine (0.906) are comparable to the LHE=0.932 for X65 [25]. This result demonstrates that molecules could contribute efficiently in sunlight absorption along with FAPbI$_3$ perovskite and result in a strong sunlight harvesting device. It is notable that SFX-Selenocysteine exhibits the lowest LHE=0.224.

Absorption spectra of HTM derivatives in dichloromethane solution are indicated in Fig. 6. Also, maximum absorbance (λ^{max}_{abs}) and emission (λ^{max}_{em}) wavelengths, Stokes shift, first singlet excitation energy (E^1), and E_b of investigated HTMs in dichloromethane are collected in Table 4. It is observed that only SFX-Selenocysteine absorption happens within visible area (λ_{abs}^{max}=800 nm) with the lowest intensity among all samples. However, absorptions of other molecules occur within UV spectral area, like Spiro-OMeTAD with main light λ^{max}_{abs}<400 nm, confirming it does not have a competion with FAPbI$_3$ for sunlight harvesting. All λ_{abs}^{max} values of HTMs (except for SFX-Selenocysteine) change from 239.23 nm (SFX-Proline) to 286.91 nm (SFX-Arginine).

Additionally, the highest and the lowest peak intensities of the absorption spectra are seen for SFX-Cysteine and SFX-Tyrosine, respectively.

Fig. 7 displays the emission PL spectra of HTM derivatives in dichloromethane. Stokes shift (λ_{ss}) stands for the difference in wavelengths of absorption UV-Vis and emission PL peaks. Consequently, bigger Stokes shifts exhibit further emission peak shifts toward lower energy (visible region) because of losing energy by absorbed photons via non-radiative or radiative processes, which diminish the emitted photons energy [47, 48]. Furthermore, the radiative PL emission can be considered as hole-electron recombination that is unfavorable for an efficient PSC. Hence, a lower PL intensity but a greater λ_{ss} are highly advantageous for PSCs because a larger λ_{ss} reveals that charge carriers recombination has a lower energy and a weaker recombination happens [49]. Again except for SFX-Selenocysteine with the unusually biggest λ_{ss}=2040.00 nm, the smallest and the largest λ_{ss} values of 31.09 and 378.40 nm are measured for SFX-Arginine and SFX-Serine respectively. Accordingly, the SFX-Serine and SFX-Selenocysteine with the largest λ_{ss} but the lowest PL intensities may be the most desirable HTMs amongst all studied materials.

Another crucial parameter is binding energy of exciton (electron-hole couple) to determine optical and electronic features of HTMs [50]. E_b is expressed by formula $E_b = E_g - E_x = \Delta(H–L) - E^1$, in which E_g bandgap is replaced by $\Delta(H–L)$ while E_x denotes optical gap that is known as first singlet excitation energy (E^1) [51]. Electron-hole binding energy exhibits their columbic attraction. A lower E_b verifies a less columbic interaction whereas improved electron-hole separation and boosted PCE. E_b values of the SFX-based samples within dichloromethane solution are given in Table 4. It is observed that SFX-Selenocysteine has the smallest E_b=0.2946 eV and among rest of molecules, the E_b values change from 0.5075 eV (in SFX-Methionine) to 0.6067 eV

(in SFX-Threonine). Overall, the SFX-Selenocysteine and SFX-Methionine are the best samples when considering the E_b values.

3.7. Infrared spectra

Fig. 8(a) provides the infrared (IR) spectra of HTM samples calculated in dichloromethane solution. It is seen that there are several peaks with diverse intensities in the IR spectra of SFX-based HTMs. Two peaks located near 1800-3200 and 3600-3850 cm^{-1} respectively reveal stretching of C–H and O–H bonds [52, 53]. Several bands nearby 1100 cm^{-1} display stretching of C–O bonds [54] while bands positioned close to 1550 and 1350 cm^{-1} display asymmetric and symmetric stretchings of C=C bonds [55]. Peaks detected between 600-800 cm^{-1} are associated with C–H bending vibrations [56]. Bands positioned at about 1650 display bending/deformation vibrations of O-H bonds [57]. Besides, bands at almost 1000 and 950 cm^{-1} illustrate stretchings of C–O and C-S bonds, respectively [58].

3.8. Reorganization energies

A HTM with larger hole mobility will exhibit boosted fill factor (FF) and greater short-circuit current density (J_{SC}) in PSCs. Using hopping theory, charge mobility can be obtained for a material. For this purpose, reorganization energy should be determined based on Marcus charge transport concept which can explain the process [59, 60]. Reorganization energy is an essential parameter that investigates charge transport characteristics of a molecule [61], which equals the energy necessary for structural distortion and modification upon charge transportation. The reorganization energy contains two parts including internal and external reorganizations [62]. The internal reorganization reveals polarization changes of in atomic geometry involved in charge

transition from neutral to ionic form and vice versa. External reorganization denotes electronic polarization changes in adjacent molecules. However, theoretical estimation of external reorganization is hard and thus it is ignored. Here, internal reorganization energy is measured to describe geometry variations of neutral and ionic molecules. The hole and electron reorganization energies (λ_h and λ_e) of HTM structures are calculated by Eqs. (12) and (13) and results are gathered in Table 5. In these formula, E_0, E_+, and E_- describe energies of neutral, cationic, and anionic species whereas E_0^*, E_+^*, and E_-^* stand for energies of minimized neutral and cationic/anionic species at cationic/anionic and neutral forms, respectively. Also, Fig. 8(b) affords changes of electron and hole reorganization energies of HTMs.

$$\lambda_h = (E_+^* - E_+) + (E_0^* - E_0) \tag{12}$$

$$\lambda_e = (E_-^* - E_-) + (E_0^* - E_0) \tag{13}$$

According to Marcus charge transport principle, a bigger reorganization energy signifies an inferior electron/hole transfer feature. From Table 5 and Fig. 8(b), it can be understood that the λ_h values of all samples (except for SFX-Serine with λ_h=1.0011 eV and λ_e=0.5692 eV) are smaller than their corresponding λ_e values, confirming they are more favorable HTMs than being used as ETMs. The λ_h values of SFX-based materials (except for SFX-Serine) vary from 0.1854 eV (in SFX-Proline) to 0.6293 eV (in SFX-Lysine). Hence, the largest hole reorganization energy is required in SFX-Serine for changing the geometry from neutral to cationic state because the largest structural distortion happens when it is varied from neutral to cationic form. Overall, it may be said that the SFX-Serine with the least λ_h value is the most ideal sample based on the hole reorganization energy data. It is expected that a smaller λ_h results in a higher hole mobility.

3.9. Charge-transfer integrals and intrinsic mobility

To calculate hole mobility, dimers of molecules with the highest stability (lowest energy) must be employed based on hole hopping theory because dimers significantly contribute to transfer pathways between molecular pairs. Crystallography parameters of SFX-based structures with the highest stability are provided in Table 6 and Fig. S3 exhibits their dimer structures used for hole mobility calculations. Also, Fig. 9 presents unit cells of SFX-based structures with the highest stability.

Charge hopping rate ($k_{h/e}$) was calculated using Eq. (14) based on Marcus theory [63], where $V_{h/e}$, K_B, and T, respectively, specify hole/electron transfer integral, Boltzmann constant, and temperature (298 K).

$$k_{h/e} = \frac{v2h/e}{\hbar} \sqrt{\frac{\pi}{\lambda h/ekBT}} \exp(\frac{-\lambda h/e}{4kBT}) \tag{14}$$

A beneficial factor in evaluating $k_{h/e}$ is charge transfer integral (V). The hole transfer integral is calculated from energy splitting of HOMO and HOMO-1 orbitals for neighboring species. This is named Energy splitting in Dimers (ESID) method. The electron transfer integral in ESID approach is obtained using LUMO and LUMO+1 orbitals [36]. Therefore, hole- and electron-transport integrals (V_h and V_e) are achieved by Eqs. (15) and (16), in which $E_{(L+1)}$, E_L, $E_{(H-1)}$, and E_H are energies of LUMO+1, LUMO, HOMO-1, and HOMO orbitals, respectively. The V_h and V_e values of SFX-based HTMs in Table 5 change in the ranges of 0.03197-0.33987 and 0.10327-1.00995 eV, respectively.

$$V_h = \frac{E_H - E_{H-1}}{2} \tag{15}$$

$$V_e = \frac{E_{L+1} - E_L}{2} \tag{16}$$

Charge mobility (μ) can be approximately calculated by Eq. (17) based on Einstein relation [64], in which r displays centroid-centroid distance.

$$\mu = \frac{e}{kBT} \sum_i r_i^2 k_i p_i \qquad (17)$$

Table 7 affords centroid-to-centroid distances (r) and hole/electron mobilities (μ_h/μ_e) of SFX-based HTM molecules in dichloromethane. As shown in Table 7, lower reorganization energy (λ) whereas greater transport integral (V) are required for enhanced charge mobility [65]. Charge mobility can greatly influence J_{SC} and FF of PSC devices [66]. Hence, we could expect changes in FF and J_{SC} of PSC comparable to μ_h value variations measured for SFX-based HTMs.

A linear relationship is observed between the k_h/k_e and μ_h/μ_e values of HTMs so that a larger charge mobility is measured for a material with a higher charge transfer rate. For most samples, the k_h and hole mobility are bigger that their related k_e and electron mobility values, which approve these compounds are more favorable transport holes compared to electrons. However, in cases of SFX-Histidine, SFX-Isoleucine, SFX-Phenylalanine, SFX-Serine, SFX-Threonine, SFX-Tryptophan, and SFX-Tyrosine, the k_h and μ_h values are smaller than the k_e and μ_e values. This result reveals that these samples are not suitable HTMs for PSCs and it may be better if they can be used as ETMs. Among all molecules, SFX-Leucine, SFX-Methionine, SFX-Proline, and SFX-Aspartic acid illustrate the greatest k_h values of 1.9763×10^{14}, 9.2983×10^{13}, 6.1004×10^{13}, and 6.2993×10^{13} s^{-1}, respectively. Also, the biggest μ_h values of 12.931, 7.4891, 5.5604, and 4.3217 cm^{2}V^{-1}s^{-1} are attained for SFX-Leucine, SFX-Methionine, SFX-Proline, and SFX-Arginine, respectively. Thus, it is found that the best HTM can be SFX-Leucine according to the μ_h data. It is noteworthy that the hole mobilities of all samples (even those with higher electron mobilities) are very much larger than (as big as 1000 times and higher) both of the calculated ($\mu_h = 5.65 \times 10^{-3}$ cm^{2}V^{-1}s^{-1}) and experimental ($\mu_h = 4.53 \times 10^{-4}$ cm^{2}V^{-1}s^{-1}) values reported for Spiro-OMeTAD [67].

This extraordinary result proves that the designed SFX-based materials are highly valuable HTMs for PSC photovoltaics and can result in high efficiencies.

3.10. Open-circuit voltage (V_{OC}) and fill factor

V_{OC} is a very significant parameter which is used to calculate solar cell efficiency. V_{OC} equals the uppermost voltage while current is zero [68, 69]. To determine V_{OC} by Eq. (18), LUMO of acceptor and HOMO of donor are used. In this formula, e=1 reveals charge of electron and constant 0.3 shows voltage decrease.

$$V_{oc} = E_{LUMO \text{ of acceptor}} - E_{HOMO \text{ of donor}} - 0.3/e \qquad (18)$$

Larger negative HOMO energies of HTM samples can show large V_{OC} for PSCs. V_{OC} value of each devised PSC is associated with difference of SnO_2 ETM conduction band (-4.5 eV) [70] and E_{HOMO} of HTM. Table 8 indicates the computed V_{OC} and FF values of PSCs containing SFX-based HTMs and SnO_2 ETM. Obviously, the largest V_{OC} values of 0.916, 0.894, 0.815, and 0.808 V are achieved for SFX-Arginine, SFX-Threonine, SFX-Proline, and SFX-Methionine, respectively. Moreover, the smallest V_{OC} values of 0.378, 0.409, 0.434, and 0.455 V for SFX-Tyrosine, SFX-Serine, SFX-Alanine, and SFX-Phenylalanine, respectively.

FF is also a critical factor that highly affects PSC performance [71, 72]. Eq. (19) has been utilized to calculate FF values of PSCs with SFX-based HTMs and SnO_2 ETM, in which e=1 is electron charge, K_B is the Boltzmann constant ($8.61733034 \times 10^{-5}$ and T=298 K is temperature.

$$FF = \frac{\frac{e\,V_{OC}}{K_B\,T} - \ln(\frac{e\,V_{OC}}{K_B\,T} + 0.72)}{\frac{e\,V_{OC}}{K_B\,T} + 1} \qquad (19)$$

Table 8 offers FFs of SFX-based HTM samples used in PSCs with SnO_2 ETM. Also, Fig. 10 demonstrates variations of E_b, V_{OC}, and FF values of HTM derivatives calculated in dichloromethane solution. It is evident that the molecules SFX-Arginine, SFX-Threonine, SFX-

Proline, and SFX-Methionine, respectively, exhibit the highest FF values of 0.875, 0.872, 0.863, and 0.862. Furthermore, the variation trend in FF values exactly follow the changes in the V_{OC} values. Notably, in addition to these four samples with FF>0.85, there are other samples with FF values greater than 0.8. Also, the lowest FF value is 0.762, which is very much larger than the values usually measured for PSCs with other SFX-based HTMs [73-75]. This result verifies that all of the devised SFX-based molecules in this study are very beneficial HTMs. Thus, considering the V_{OC} and FF values, SFX-Arginine can be chosen as the most satisfactory HTM for PSCs with SFX-based HTMs and SnO_2 ETM.

4. Conclusions

In this effort, hole transport materials were designed based on SFX core and 21 natural amino acids as eco-friendly green substituents. Crystal and molecular structures, optoelectronic features, and hole mobilities of HTMs were examined through DFT computations. It was revealed that among 21 samples, HOMO energies of 17 derivatives were suitable for hole transfer process. All SFX-based molecules had higher negative chemical potentials than standard HTMs such as X65 with μ=-2.46 eV and Spiro-OMeTAD (μ=-2.719 eV, η=1.782 eV, S=0.561 eV), signifying they had a higher stability compared to these famous HTMs. The biggest μ_h values of 12.931, 7.4891, 5.5604, and 4.3217 $cm^2V^{-1}s^{-1}$ were measured for SFX-Leucine, SFX-Methionine, SFX-Proline, and SFX-Arginine, respectively. Furthermore, the largest FF and V_{OC} values were attained for SFX-Arginine, SFX-Threonine, SFX-Proline, and SFX-Methionine. Importantly, all of FF values were >0.76, which were very much larger than the values usually measured for PSCs with other SFX-based HTMs, substantiating all of the devised SFX-based molecules were very advantageous HTMs. Last but not least, SFX-amino acid materials exhibited unique features for employment as

eco-friendly, green, inexpensive, and proficient HTMs and appropriate alternatives for the expensive Spiro-OMeTAD HTM.

Conflicts of interest

Authors declare that there are not any personal or financial conflicts of interest.

Data availability

All data will be delivered on request.

References

[1] B. Chen, N. Ren, Y. Li, L. Yan, S. Mazumdar, Y. Zhao, X. Zhang, Insights into the Development of Monolithic Perovskite/Silicon Tandem Solar Cells, Advanced Energy Materials 12(4) (2022) 2003628.

[2] H. Chen, S. Teale, B. Chen, Y. Hou, L. Grater, T. Zhu, K. Bertens, S.M. Park, H.R. Atapattu, Y. Gao, M. Wei, A.K. Johnston, Q. Zhou, K. Xu, D. Yu, C. Han, T. Cui, E.H. Jung, C. Zhou, W. Zhou, A.H. Proppe, S. Hoogland, F. Laquai, T. Filleter, K.R. Graham, Z. Ning, E.H.

Sargent, Quantum-size-tuned heterostructures enable efficient and stable inverted perovskite solar cells, Nature Photonics 16(5) (2022) 352-358.

[3] T.J. Jacobsson, A. Hultqvist, A. García-Fernández, A. Anand, A. Al-Ashouri, A. Hagfeldt, A. Crovetto, A. Abate, A.G. Ricciardulli, A. Vijayan, A. Kulkarni, A.Y. Anderson, B.P. Darwich, B. Yang, B.L. Coles, C.A.R. Perini, C. Rehermann, D. Ramirez, D. Fairen-Jimenez, D. Di Girolamo, D. Jia, E. Avila, E.J. Juarez-Perez, F. Baumann, F. Mathies, G.S.A. González, G. Boschloo, G. Nasti, G. Paramasivam, G. Martínez-Denegri, H. Näsström, H. Michaels, H. Köbler, H. Wu, I. Benesperi, M.I. Dar, I. Bayrak Pehlivan, I.E. Gould, J.N. Vagott, J. Dagar, J. Kettle, J. Yang, J. Li, J.A. Smith, J. Pascual, J.J. Jerónimo-Rendón, J.F. Montoya, J.-P. Correa-Baena, J. Qiu, J. Wang, K. Sveinbjörnsson, K. Hirselandt, K. Dey, K. Frohna, L. Mathies, L.A. Castriotta, M.H. Aldamasy, M. Vasquez-Montoya, M.A. Ruiz-Preciado, M.A. Flatken, M.V. Khenkin, M. Grischek, M. Kedia, M. Saliba, M. Anaya, M. Veldhoen, N. Arora, O. Shargaieva, O. Maus, O.S. Game, O. Yudilevich, P. Fassl, Q. Zhou, R. Betancur, R. Munir, R. Patidar, S.D. Stranks, S. Alam, S. Kar, T. Unold, T. Abzieher, T. Edvinsson, T.W. David, U.W. Paetzold, W. Zia, W. Fu, W. Zuo, V.R.F. Schröder, W. Tress, X. Zhang, Y.-H. Chiang, Z. Iqbal, Z. Xie, E. Unger, An open-access database and analysis tool for perovskite solar cells based on the FAIR data principles, Nature Energy 7(1) (2022) 107-115.

[4] W. Ali Zahid, W. Akram, M. Fiaz Ahmad, K. Ayub, J. Iqbal, Designing of dimethylfluorene-based hole transport materials for high-performance organic/perovskite solar cells, Solar Energy 262 (2023) 111888.

[5] N. Chawki, M. Rouchdi, M. Alla, B. Fares, Simulation and analysis of high-performance hole transport material SrZrS3-based perovskite solar cells with a theoretical efficiency approaching 26%, Solar Energy 262 (2023) 111913.

[6] Z. Shariatinia, How does changing substituents affect the hole transport characteristic of butterfly-shaped materials based on fluorene–dithiophene core for perovskite photovoltaics, Journal of Industrial and Engineering Chemistry 118 (2023) 280-297.

[7] R. Azmi, E. Ugur, A. Seitkhan, F. Aljamaan, A.S. Subbiah, J. Liu, G.T. Harrison, M.I. Nugraha, M.K. Eswaran, M. Babics, Damp heat–stable perovskite solar cells with tailored-dimensionality 2D/3D heterojunctions, Science 376(6588) (2022) 73-77.

[8] L. Yang, J. Feng, Z. Liu, Y. Duan, S. Zhan, S. Yang, K. He, Y. Li, Y. Zhou, N. Yuan, J. Ding, S. Liu, Record-Efficiency Flexible Perovskite Solar Cells Enabled by Multifunctional Organic Ions Interface Passivation, Advanced Materials 34(24) (2022) 2201681.

[9] R. Hussain, M. Adnan, K. Atiq, M. Usman Khan, Z. H. Farooqi, J. Iqbal, R. Begum, Designing of silolothiophene-linked triphenylamine-based hole transporting materials for perovskites and donors for organic solar cells-A DFT study, Solar Energy 253 (2023) 187-198.

[10] F. Mohamadkhani, M. Heidariramsheh, S. Javadpour, E. Ghavaminia, S.M. Mahdavi, N. Taghavinia, Sb2S3 and Cu3SbS4 nanocrystals as inorganic hole transporting materials in perovskite solar cells, Solar Energy 223 (2021) 106-112.

[11] F. Fu, J. Li, T.C.J. Yang, H. Liang, A. Faes, Q. Jeangros, C. Ballif, Y. Hou, Monolithic Perovskite-Silicon Tandem Solar Cells: From the Lab to Fab?, Advanced Materials (2022) 2106540.

[12] L. Noori, V. Hoseinpour, Z. Shariatinia, Optimization of TiO2 paste concentration employed as electron transport layers in fully ambient air processed perovskite solar cells with a low-cost architecture, Ceramics International 48(1) (2022) 320-336.

[13] P.-K. Kung, M.-H. Li, P.-Y. Lin, Y.-H. Chiang, C.-R. Chan, T.-F. Guo, P. Chen, A Review of Inorganic Hole Transport Materials for Perovskite Solar Cells, Advanced Materials Interfaces 5(22) (2018) 1800882.

[14] M. Maciejczyk, A. Ivaturi, N. Robertson, SFX as a low-cost 'Spiro' hole-transport material for efficient perovskite solar cells, Journal of Materials Chemistry A 4(13) (2016) 4855-4863.

[15] L. Wang, F. Zhang, T. Liu, W. Zhang, Y. Li, B. Cai, L. He, Y. Guo, X. Yang, B. Xu, A crosslinked polymer as dopant-free hole-transport material for efficient nip type perovskite solar cells, Journal of Energy Chemistry 55 (2021) 211-218.

[16] C.-S. Li, B.-Y. Ren, Y.-G. Sun, Low-cost and stable SFX-based semiconductor materials in organic optoelectronics, Resources Chemicals and Materials 2(1) (2023) 100-109.

[17] F. Bischoff, H. Adkins, THE CONDENSATION OF DIPHENIC ANHYDRIDE WITH RESORCINOL, Journal of the American Chemical Society 45(4) (1923) 1030-1033.

[18] L.-H. Xie, F. Liu, C. Tang, X.-Y. Hou, Y.-R. Hua, Q.-L. Fan, W. Huang, Unexpected One-Pot Method to Synthesize Spiro[fluorene-9,9'-xanthene] Building Blocks for Blue-Light-Emitting Materials, Organic Letters 8(13) (2006) 2787-2790.

[19] M. Sun, R. Xu, L. Xie, Y. Wei, W. Huang, Toward Eco-friendly Green Organic Semiconductors: Recent Advances in Spiro [fluorene-9, 9′-xanthene](SFX)-Based Optoelectronic Materials and Devices, Chinese Journal of Chemistry 33(8) (2015) 815-827.

[20] A. Alizadeh, M. Roudgar-Amoli, S.-M. Bonyad-Shekalgourabi, Z. Shariatinia, M. Mahmoudi, F. Saadat, Dye sensitized solar cells go beyond using perovskite and spinel inorganic materials: A review, Renewable and Sustainable Energy Reviews 157 (2022) 112047.

[21] Z. Li, Y. Yun, H. Huang, Z. Ding, X. Li, B. Zhao, W. Huang, Fluorine substitution position effects on spiro (fluorene-9, 9′-xanthene) cored hole transporting materials for high-performance planar perovskite solar cells, Journal of Energy Chemistry 57 (2021) 341-350.

[22] Z. Shariatinia, Designing novel spiro compounds as favorable hole transport materials for quantum dot sensitized photovoltaics, Solar Energy 236 (2022) 548-560.

[23] B.M. Trost, The atom economy—a search for synthetic efficiency, Science 254(5037) (1991) 1471-1477.

[24] Y. Hayashi, Time and pot economy in total synthesis, Accounts of Chemical Research 54(6) (2021) 1385-1398.

[25] S. Gul, K.M. Katubi, I.A. Bhatti, J. Iqbal, M. Al-Buriahi, S. Alomairy, Tuning the photovoltaic parameters of spiro [fluorenexanthene]-diol (SFX-OH)-based crosslinked donor materials for efficient organic solar cells, Computational and Theoretical Chemistry 1214 (2022) 113778.

[26] R.A. Marcus, Electron transfer reactions in chemistry: theory and experiment (Nobel lecture), Angewandte Chemie International Edition in English 32(8) (1993) 1111-1121.

[27] W.-Q. Deng, L. Sun, J.-D. Huang, S. Chai, S.-H. Wen, K.-L. Han, Quantitative prediction of charge mobilities of π-stacked systems by first-principles simulation, Nature protocols 10(4) (2015) 632-642.

[28] M. Vatanparast, Z. Shariatinia, Isoindigo derivatives as promising hole transport materials for perovskite solar cells, Solar Energy 230 (2021) 260-268.

[29] G. Pindolia, S. Shinde, P.K. Jha, P3CPenT as an organic hole transport layer for perovskite solar cells, International Journal of Quantum Chemistry 123(18) (2023) e27149.

[30] H. Liu, H. Sun, Q. Chen, F. Wu, X. Liu, Two simple hole-transporting materials for perovskite solar cells: A DFT calculation and experimental study, Applied Surface Science 604 (2022) 154603.

[31] Q. Chen, H. Liu, R. Wang, C. Wu, F. Wu, X. Liu, X. Liu, Peripheral group engineering on hole-transporting materials in perovskite solar cells: Theoretical design and experimental research, Dyes and Pigments 206 (2022) 110604.

[32] S. Naqvi, A. Patra, Hole transport materials for perovskite solar cells: a computational study, Materials Chemistry and Physics 258 (2021) 123863.

[33] C.-G. Zhan, J.A. Nichols, D.A. Dixon, Ionization potential, electron affinity, electronegativity, hardness, and electron excitation energy: molecular properties from density functional theory orbital energies, The Journal of Physical Chemistry A 107(20) (2003) 4184-4195.

[34] G. Malloci, G. Cappellini, G. Mulas, A. Mattoni, Electronic and optical properties of families of polycyclic aromatic hydrocarbons: A systematic (time-dependent) density functional theory study, Chemical Physics 384(1-3) (2011) 19-27.

[35] S.S. Zade, M. Bendikov, From oligomers to polymer: convergence in the HOMO− LUMO gaps of conjugated oligomers, Organic letters 8(23) (2006) 5243-5246.

[36] T.P. Nguyen, J.H. Shim, J.Y. Lee, Density functional theory studies of hole mobility in picene and pentacene crystals, The Journal of Physical Chemistry C 119(21) (2015) 11301-11310.

[37] Z.-Z. Sun, Y.-L. Xu, W.-L. Ding, W.-J. Chi, How to stabilize the HOMO levels and to improve the charge transport properties of hole-transporting materials? Introducing a symmetrical core unit, Synthetic Metals 247 (2019) 157-162.

[38] F. Ma, J. Li, W. Li, N. Lin, L. Wang, J. Qiao, Stable α/δ phase junction of formamidinium lead iodide perovskites for enhanced near-infrared emission, Chemical science 8(1) (2017) 800-805.

[39] Z. Shariatinia, S.-I. Sarmalek, Molecular engineering of several butterfly-shaped hole transport materials containing dibenzo[b,d]thiophene core for perovskite photovoltaics, Scientific Reports 12(1) (2022) 13954.

[40] M. Hao, D. Tan, W. Chi, Z.-s. Li, A π-extended triphenylamine based dopant-free hole-transporting material for perovskite solar cells via heteroatom substitution, Physical Chemistry Chemical Physics 24(7) (2022) 4635-4643.

[41] I.M. Abdellah, E. Yildirim, A. El-Shafei, Low-cost novel X-shaped hole transport materials for efficient perovskite solar cells: Molecular modelling of the core and schiff base effects on photovoltaic and photophysical properties, Materials Chemistry and Physics 296 (2023) 127188.

[42] A.F. Latypova, A.V. Maskaev, L.G. Gutsev, N.A. Emelianov, I.E. Kuznetsov, P.M. Kuznetsov, S.L. Nikitenko, Y.V. Baskakova, A.V. Akkuratov, E.A. Komissarova, L.A. Frolova, S.M. Aldoshin, P.A. Troshin, Side chain engineering and film uniformity: two key parameters for the rational design of dopant-free polymeric hole transport materials for efficient and stable perovskite solar cells, Materials Today Chemistry 26 (2022) 101218.

[43] M. Vatanparast, Z. Shariatinia, Efficient hole transport materials based on naphthyridine core designed for application in perovskite solar photovoltaics, Journal of Molecular Graphics and Modelling 117 (2022) 108292.

[44] J.-J. Guo, Z.-C. Bai, X.-F. Meng, M.-M. Sun, J.-H. Song, Z.-S. Shen, N. Ma, Z.-L. Chen, F. Zhang, Novel dopant-free metallophthalocyanines based hole transporting materials for perovskite solar cells: The effect of core metal on photovoltaic performance, Solar Energy 155 (2017) 121-129.

[45] H.A. Malik, L. Ma, J. Luo, J. Xia, Z. Wan, M.K. Khan, X. Shao, C. Jia, Novel hole transporting material based on tetrathiafulvalene derivative: A step towards dopant free, ambient stable and efficient perovskite solar cells, Solar Energy 201 (2020) 658-665.

[46] N. Naeem, R.A. Shehzad, M. Ans, M.S. Akhter, J. Iqbal, Dopant free triphenylamine-based hole transport materials with excellent photovoltaic properties for high-performance perovskite solar cells, Energy Technology 10(2) (2022) 2100838.

[47] F. Abbas, M.D. Mohammadi, H. Louis, I.O. Amodu, D.E. Charlie, T.E. Gber, Design of new bithieno thiophene (BTTI) central core-based small molecules as efficient hole transport materials for perovskite solar cells and donor materials for organic solar cells, Materials Science and Engineering: B 291 (2023) 116392.

[48] J.-L. Brédas, D. Beljonne, V. Coropceanu, J. Cornil, Charge-transfer and energy-transfer processes in π-conjugated oligomers and polymers: a molecular picture, Chemical reviews 104(11) (2004) 4971-5004.

[49] J.M. Dos Santos, L.K. Jagadamma, M. Cariello, I.D. Samuel, G. Cooke, A BODIPY small molecule as hole transporting material for efficient perovskite solar cells, Sustainable Energy & Fuels 6(18) (2022) 4322-4330.

[50] W. Akram, W.A. Zahid, L.A. El Maati, R. Altuijri, I. Hossain, M.S. Akhter, J. Iqbal, Engineering push–pull structural versatility in highly functional carbazole-based hole transporting materials design for efficient perovskites solar devices, Journal of Photochemistry and Photobiology A: Chemistry 444 (2023) 114991.

[51] Z. Shariatinia, Hole transport properties of some spiro-based materials for quantum dot sensitized solar devices, Journal of Photochemistry and Photobiology A: Chemistry 427 (2022) 113810.

[52] Z. Nikfar, Z. Shariatinia, Phosphate functionalized (4,4)-armchair CNTs as novel drug delivery systems for alendronate and etidronate anti-osteoporosis drugs, Journal of Molecular Graphics and Modelling 76 (2017) 86-105.

[53] K. Gholivand, M. Pourayoubi, Z. Shariatinia, 2,3J(P,X) [X=H, C] coupling constants dependency on the ring size, hybridization and substituents in new diazaphospholes and diazaphosphorinanes, NMR and X-ray crystallography studies, Polyhedron 26(4) (2007) 837-844.

[54] M.S. Zoromba, H. Maddah, M. Abdel-Aziz, A.F. Al-Hossainy, Physical structure, TD-DFT computations, and optical properties of hybrid nanocomposite thin film as optoelectronic devices, Journal of Industrial and Engineering Chemistry 112 (2022) 106-124.

[55] L. Andrews, A. Citra, Infrared spectra and density functional theory calculations on transition metal nitrosyls. Vibrational frequencies of unsaturated transition metal nitrosyls, Chemical reviews 102(4) (2002) 885-912.

[56] Z. Nikfar, Z. Shariatinia, DFT computational study on the phosphate functionalized SWCNTs as efficient drug delivery systems for anti-osteoporosis zolendronate and risedronate drugs, Physica E: Low-dimensional Systems and Nanostructures 91 (2017) 41-59.

[57] Z. Shariatinia, Chapter 2 - Pharmaceutical applications of natural polysaccharides, in: M.S. Hasnain, A.K. Nayak (Eds.), Natural Polysaccharides in Drug Delivery and Biomedical Applications, Academic Press2019, pp. 15-57.

[58] K. Gholivand, Z. Shariatinia, Two conformers in the solid state for a novel organotin(IV) complex of a phosphoramidate: Syntheses, spectroscopic study and crystal structures of

several new organotin(IV) complexes of N-benzoylphosphoric triamides, Journal of Organometallic Chemistry 691(20) (2006) 4215-4224.

[59] S. Zahid, A. Rasool, M. Ans, M. Salim Akhter, J. Iqbal, M.S. Al-Buriahi, S. Alomairy, Z.A. Alrowaili, Environmentally compatible and highly improved hole transport materials (HTMs) based on benzotrithiophene (BTT) skeleton for perovskite as well as narrow bandgap donors for organic solar cells, Solar Energy 231 (2022) 793-808.

[60] Q. Wang, Z. Zeng, Y. Li, X. Chen, Efficient strategies for improving the performance of EDOT derivatives and TPA derivatives-based hole transport materials for perovskite solar cells, Solar Energy 208 (2020) 10-19.

[61] W. Zhu, K. Zhou, Y. Fo, Y. Li, B. Guo, X. Zhang, X. Zhou, Rational design of small molecule hole-transporting materials with a linear π-bridge for highly efficient perovskite solar cells, Physical Chemistry Chemical Physics 24(31) (2022) 18793-18804.

[62] H. Ashassi-Sorkhabi, P. Salehi-Abar, How the change of OMe substituent position affects the performance of spiro-OMeTAD in neutral and oxidized forms: theoretical approaches, RSC Advances 8(33) (2018) 18234-18242.

[63] R.A. Marcus, Chemical and electrochemical electron-transfer theory, Annual review of physical chemistry 15(1) (1964) 155-196.

[64] J. Xiao, H.-J. Yu, D. Wang, W.-J. Gao, A. Shinohara, J. Xia, G. Shao, An Acetylene-Linked 9,9′-Bicarbazole-Based Hole-Transporting Material for Efficient Perovskite Solar Cells, Energy & Fuels 36(4) (2022) 2086-2094.

[65] W.-Q. Deng, W.A. Goddard, Predictions of Hole Mobilities in Oligoacene Organic Semiconductors from Quantum Mechanical Calculations, The Journal of Physical Chemistry B 108(25) (2004) 8614-8621.

[66] K.-M. Lee, Y.-S. Huang, W.-H. Chiu, Y.-K. Huang, G. Chen, G.B. Adugna, S.-R. Li, F.-J. Lin, S.-I. Lu, H.-C. Hsieh, K.-L. Liau, C.-C. Huang, Y. Tai, Y.-T. Tao, Y.-D. Lin, Fluorinated Pentafulvalene-Fused Hole-Transporting Material Enhances the Performance of Perovskite Solar Cells with Efficiency Exceeding 23%, Advanced Functional Materials n/a(n/a) 2306367.

[67] W.-J. Chi, Q.-S. Li, Z.-S. Li, Exploring the electrochemical properties of hole transport materials with spiro-cores for efficient perovskite solar cells from first-principles, Nanoscale 8(11) (2016) 6146-6154.

[68] E. Jalali-Moghadam, Z. Shariatinia, Al3+ doping into TiO2 photoanodes improved the performances of amine anchored CdS quantum dot sensitized solar cells, Materials Research Bulletin 98 (2018) 121-132.

[69] F. Ziaeifar, A. Alizadeh, Z. Shariatinia, Dye sensitized solar cells fabricated based on nanocomposite photoanodes of TiO2 and AlMo0.5O3 perovskite nanoparticles, Solar Energy 218 (2021) 435-444.

[70] L. Xiong, Y. Guo, J. Wen, H. Liu, G. Yang, P. Qin, G. Fang, Review on the Application of SnO2 in Perovskite Solar Cells, Advanced Functional Materials 28(35) (2018) 1802757.

[71] E. Jalali-Moghadam, Z. Shariatinia, Quantum dot sensitized solar cells fabricated by means of a novel inorganic spinel nanoparticle, Applied Surface Science 441 (2018) 1-11.

[72] Z. Zolfaghari-Isavandi, Z. Shariatinia, Fabrication of CdS quantum dot sensitized solar cells using nitrogen functionalized CNTs/TiO2 nanocomposites, Diamond and Related Materials 81 (2018) 1-15.

[73] J. Zhang, B. Xu, L. Yang, C. Ruan, L. Wang, P. Liu, W. Zhang, N. Vlachopoulos, L. Kloo, G. Boschloo, L. Sun, A. Hagfeldt, E.M.J. Johansson, The Importance of Pendant Groups on Triphenylamine-Based Hole Transport Materials for Obtaining Perovskite Solar Cells with over 20% Efficiency, Advanced Energy Materials 8(2) (2018) 1701209.

[74] Y. Fu, Y. Li, Q. Zeng, H. Wu, L. Wang, H. Tang, G. Xing, D. Cao, Influence of donor units on spiro[fluorene-9,9′-xanthene]-based dopant-free hole transporting materials for perovskite solar cells, Solar Energy 216 (2021) 180-187.

[75] B. Xu, D. Bi, Y. Hua, P. Liu, M. Cheng, M. Grätzel, L. Kloo, A. Hagfeldt, L. Sun, A low-cost spiro[fluorene-9,9′-xanthene]-based hole transport material for highly efficient solid-state dye-sensitized solar cells and perovskite solar cells, Energy & Environmental Science 9(3) (2016) 873-877.

Table 1. HOMO, LUMO, E_g, $E_{binding}$ values, and dipole moments of HTMs containing natural amino acid substituents attached to para positions of aromatic rings of SFX core via nitrogen atom of NH group in dichloromethane solvent.

HTM	E(HOMO) (eV)	E(LUMO) (eV)	E_g (eV)	$E_{binding}$ (kcal/mol)	dipole moment (Debye)
SFX-Alanine	-5.233	-0.909	4.324	-7543.882	6.032
SFX-Arginine	-5.668	-1.444	4.224	-10388.149	2.065
SFX-Asparagine	-5.747	-1.121	4.625	-8449.783	3.852
SFX-Aspartic acid	-5.283	-1.004	4.280	-8309.805	3.187
SFX-Cysteine	-5.322	-0.961	4.361	-7644.639	1.806
SFX-Glutamic acid	-5.854	-1.312	4.542	-8886.650	3.985
SFX-Glutamine	-5.851	-1.362	4.490	-9352.474	8.167
SFX-Glycine	-5.205	-0.891	4.314	-6952.426	2.715
SFX-Histidine	-5.323	-1.021	4.301	-9212.496	8.516
SFX-Isoleucine	-5.456	-1.057	4.399	-9289.136	5.133
SFX-Leucine	-5.142	-0.953	4.188	-9304.235	4.108
SFX-Lysine	-5.451	-0.862	4.589	-9662.260	7.084
SFX-Methionine	-5.324	-1.306	4.017	-8807.953	2.966
SFX-Phenylalanine	-5.273	-0.960	4.313	-10038.958	6.371
SFX-Proline	-5.623	-0.917	4.706	-8431.769	6.678
SFX-Selenocysteine	-5.430	-4.977	0.453	-6590.435	5.690
SFX-Serine	-5.247	-0.861	4.386	-7711.544	6.251
SFX-Threonine	-5.652	-1.069	4.583	-8313.968	5.775
SFX-Tryptophan	-5.344	-1.035	4.309	-11030.720	4.080
SFX-Tyrosine	-5.225	-0.961	4.264	-10245.602	4.320
SFX-Valine	-3.817	-2.637	1.180	-8737.416	8.388

Table 2. Quantum chemical descriptors for investigated HTMs.

HTM	μ (eV)	η (eV)	S (eV)	χ (eV)	ω (eV)	ΔN_{max}
SFX-Alanine	-3.072	2.162	0.4625	3.072	10.199	1.421
SFX-Arginine	-3.556	2.112	0.4735	3.556	13.350	1.684
SFX-Aspartic acid	-3.143	2.140	0.4673	3.143	10.571	1.469
SFX-Cysteine	-3.141	2.181	0.4586	3.141	10.759	1.440
SFX-Glycine	-3.048	2.157	0.4636	3.048	10.021	1.413
SFX-Histidine	-3.172	2.151	0.4650	3.172	10.819	1.475
SFX-Isoleucine	-3.256	2.199	0.4547	3.256	11.660	1.481
SFX-Leucine	-3.048	2.094	0.4775	3.048	9.724	1.455
SFX-Lysine	-3.157	2.294	0.4358	3.157	11.431	1.376
SFX-Methionine	-3.315	2.009	0.4979	3.315	11.037	1.650
SFX-Phenylalanine	-3.117	2.156	0.4637	3.117	10.473	1.445
SFX-Proline	-3.270	2.353	0.4250	3.270	12.580	1.390
SFX-Selenocysteine	-5.204	0.226	4.4170	5.204	3.065	22.984
SFX-Serine	-3.054	2.193	0.4560	3.054	10.227	1.393
SFX-Threonine	-3.360	2.292	0.4364	3.360	12.937	1.466
SFX-Tryptophan	-3.189	2.154	0.4642	3.189	10.956	1.480
SFX-Tyrosine	-3.093	2.132	0.4691	3.093	10.199	1.451
Spiro-OMeTAD	-2.719	1.782	0.561	2.719	2.075	1.526

Table 3. IP, EA, f^{max}_{abs}, and LHE values for investigated HTMs.

HTM	IP (eV)	EA (eV)	f_{abs}^{max}	LHE
SFX-Alanine	5.275	1.067	1.026	0.906
SFX-Arginine	5.689	2.565	0.479	0.668
SFX-Aspartic acid	5.324	1.156	0.647	0.775
SFX-Cysteine	5.359	1.145	1.137	0.927
SFX-Glycine	5.245	1.035	0.444	0.640
SFX-Histidine	5.356	1.164	0.975	0.894
SFX-Isoleucine	5.517	2.673	0.459	0.652
SFX-Leucine	5.240	2.050	0.258	0.448
SFX-Lysine	5.528	1.347	0.314	0.514
SFX-Methionine	5.382	2.331	0.258	0.448
SFX-Phenylalanine	5.309	1.114	0.632	0.767
SFX-Proline	5.665	2.281	0.304	0.503
SFX-Selenocysteine	5.124	15.043	0.110	0.224
SFX-Serine	5.286	1.232	0.735	0.816
SFX-Threonine	5.706	2.049	0.383	0.586
SFX-Tryptophan	5.341	1.734	0.316	0.517
SFX-Tyrosine	5.259	1.119	0.605	0.752

Table 4. Wavelengths of maximum absorbance (λ^{max}_{abs}) and emission (λ^{max}_{em}), Stokes shift (λ_{ss}), first singlet excitation energy (E^1), and E_b of investigated HTMs in dichloromethane.

HTM	λ_{abs}^{max} (nm)	λ_{em}^{max} (nm)	λ_{ss} (nm)	E^1 (eV)	E_b (eV)
SFX-Alanine	248.94	313.50	64.56	3.7690	0.5549
SFX-Arginine	286.91	318.00	31.09	3.6605	0.5633
SFX-Aspartic acid	251.86	356.20	104.34	3.7216	0.5579
SFX-Cysteine	250.12	356.00	105.88	3.8033	0.5581
SFX-Glycine	247.82	357.20	109.38	3.7509	0.5632
SFX-Histidine	252.33	359.55	107.22	3.7377	0.5636
SFX-Isoleucine	256.21	310.70	54.49	3.8184	0.5803
SFX-Leucine	242.70	307.90	65.20	3.6199	0.5682
SFX-Lysine	262.86	306.35	43.49	4.0017	0.5872
SFX-Methionine	271.73	305.50	33.77	3.5097	0.5075
SFX-Phenylalanine	249.96	354.75	104.79	3.7466	0.5661
SFX-Proline	239.23	371.90	132.67	4.0914	0.6145
SFX-Selenocysteine	800.00	2840.00	2040.00	0.1582	0.2946
SFX-Serine	247.38	625.78	378.40	3.8370	0.5487
SFX-Threonine	260.19	358.50	98.31	3.9765	0.6067
SFX-Tryptophan	268.43	356.70	88.27	3.7610	0.5477
SFX-Tyrosine	249.62	367.10	117.48	3.7283	0.5355

Table 5. Hole/electron reorganization energies and V_h/V_e for investigated HTMs.

HTM	λ_h (eV)	λ_e (eV)	$|V_h|$ (eV)	$|V_e|$ (eV)
SFX-Alanine	0.3371	0.4047	0.16082	0.22327
SFX-Arginine	0.2000	0.5275	0.08980	0.22191
SFX-Aspartic acid	0.2568	0.3723	0.14871	0.26218
SFX-Cysteine	0.3329	0.4190	0.16245	0.24694
SFX-Glycine	0.2899	0.3648	0.14613	0.21647
SFX-Histidine	0.3630	0.3495	0.14245	0.27320
SFX-Isoleucine	0.3193	0.3526	0.19320	0.25606
SFX-Leucine	0.2984	0.3990	0.33987	0.21062
SFX-Lysine	0.6293	0.7484	0.15429	0.10327
SFX-Methionine	0.3287	0.3934	0.27647	0.32722
SFX-Phenylalanine	0.3215	0.3639	0.14980	0.24068
SFX-Proline	0.1854	0.3629	0.09864	0.19497
SFX-Selenocysteine	0.5114	2.9761	0.16136	1.00995
SFX-Serine	1.0011	0.5692	0.18735	0.20422
SFX-Threonine	0.3157	0.3323	0.09279	0.26041
SFX-Tryptophan	0.2924	0.3475	0.03197	0.25864
SFX-Tyrosine	0.3401	0.3634	0.20436	0.25171

Table 6. Crystallography information crystal structures of SFX-based HTMs with the highest stability.

HTM	Space group	Length a (Å)	Length b (Å)	Length c (Å)	Angle α (°)	Angle β (°)	Angle γ (°)
SFX-Alanine	P212121	19.701	12.668	10.312	90	90	90
SFX-Arginine	P-1	11.524	18.670	8.538	100.465	92.053	93.537
SFX-Aspartic acid	P21	13.325	11.520	12.853	90	129.367	90
SFX-Cysteine	P-1	15.495	12.537	11.711	134.565	104.358	95.576
SFX-Glycine	P-1	9.120	19.926	7.947	74.177	86.939	56.129
SFX-Histidine	P-1	14.531	19.641	8.143	88.942	91.931	134.696
SFX-Isoleucine	P-1	12.318	18.507	10.175	65.352	71.725	56.563
SFX-Leucine	P-1	14.963	7.454	17.326	63.296	87.479	87.685
SFX-Lysine	P21/C	15.736	18.101	12.968	90	107.284	90
SFX-Methionine	P-1	19.935	7.728	12.415	108.655	102.564	103.160
SFX-Phenylalanine	P-1	9.374	13.750	15.889	63.044	71.005	85.045
SFX-Proline	P-1	7.422	21.593	9.137	84.580	83.059	76.056
SFX-Selenocysteine	P21/C	18.975	17.928	7.973	90	91.829	90
SFX-Serine	P-1	12.875	14.330	9.502	66.124	55.208	65.696
SFX-Threonine	P212121	10.671	21.798	13.104	90	90	90
SFX-Tryptophan	P21	16.498	9.212	14.773	90	56.515	90
SFX-Tyrosine	P-1	8.428	25.052	10.509	61.235	104.367	97.501

Table 7. Centroid-to-centroid distances (r), hole/electron transfer rates (k_h/k_e),

and hole/electron mobilities (μ_h/μ_e) of SFX-based HTM molecules in dichloromethane.

HTM	r (Å)	k_h (s^{-1})	k_e (s^{-1})	μ_h (cm^{2}V^{-1}s^{-1})	μ_e (cm^{2}V^{-1}s^{-1})
SFX-Alanine	8.319	2.8636×10^{13}	2.6222×10^{13}	1.2772	1.1696
SFX-Arginine	12.396	4.3638×10^{13}	6.9199×10^{12}	4.3217	0.6853
SFX-Aspartic acid	6.757	6.1004×10^{13}	5.155×10^{13}	1.7951	1.5169
SFX-Cysteine	11.233	3.0618×10^{13}	2.7462×10^{13}	2.4899	2.2333
SFX-Glycine	9.705	4.0226×10^{13}	3.8166×10^{13}	2.4418	2.3168
SFX-Histidine	13.402	1.6863×10^{13}	7.2029×10^{13}	1.9520	8.3381
SFX-Isoleucine	6.399	5.0445×10^{13}	6.1102×10^{13}	1.3312	1.6125
SFX-Leucine	10.076	1.9763×10^{14}	2.4832×10^{13}	12.931	1.6248
SFX-Lysine	14.119	1.1452×10^{12}	1.4864×10^{11}	0.1471	0.0191
SFX-Methionine	11.179	9.2983×10^{13}	6.3698×10^{13}	7.4891	5.1304
SFX-Phenylalanine	10.133	2.9594×10^{13}	4.7663×10^{13}	1.9584	3.1541
SFX-Proline	11.703	6.2993×10^{13}	3.1640×10^{13}	5.5604	2.7928
SFX-Selenocysteine	7.190	4.3405×10^{12}	3.1624×10^{3}	0.1446	1.0536×10^{-10}
SFX-Serine	8.672	3.6761×10^{10}	3.7689×10^{12}	0.0018	0.1827
SFX-Threonine	11.152	1.2125×10^{13}	7.9255×10^{13}	0.9719	6.3526
SFX-Tryptophan	9.068	1.8742×10^{12}	6.6025×10^{13}	0.0993	3.4990
SFX-Tyrosine	10.031	4.4726×10^{13}	5.2409×10^{13}	2.9005	3.3987

Table 8. Computed V_{OC} and FF values of PSCs containing SFX-based HTMs and SnO_2 ETM.

HTM	V_{OC} (V)	FF
SFX-Alanine	0.434	0.784
SFX-Arginine	0.916	0.875
SFX-Aspartic acid	0.600	0.828
SFX-Cysteine	0.528	0.812
SFX-Glycine	0.470	0.796
SFX-Histidine	0.613	0.831
SFX-Isoleucine	0.791	0.860
SFX-Leucine	0.542	0.815
SFX-Lysine	0.675	0.842
SFX-Methionine	0.808	0.862
SFX-Phenylalanine	0.455	0.791
SFX-Proline	0.815	0.863
SFX-Selenocysteine	0.683	0.844
SFX-Serine	0.409	0.775
SFX-Threonine	0.894	0.872
SFX-Tryptophan	0.705	0.847
SFX-Tyrosine	0.378	0.762
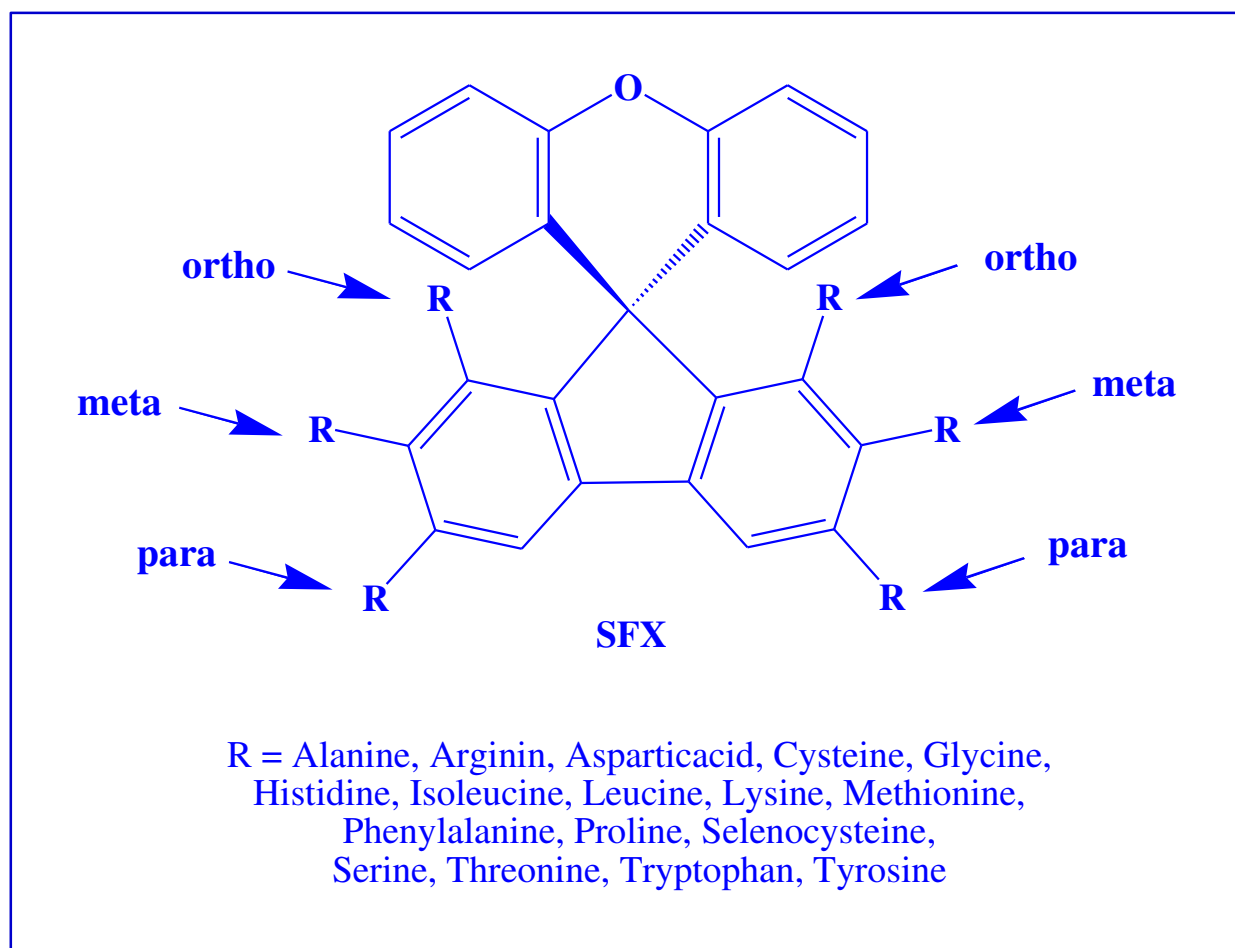
Fig. 1. SFX structure substituted with 21 natural aminoacids at ortho, metal, or papa positions of aromatic rings, in which oxygen or nitrogen atoms of terminal NH or C(O)OH groups in aminoacids are attached to the SFX core and form C-O or C-N bonds.
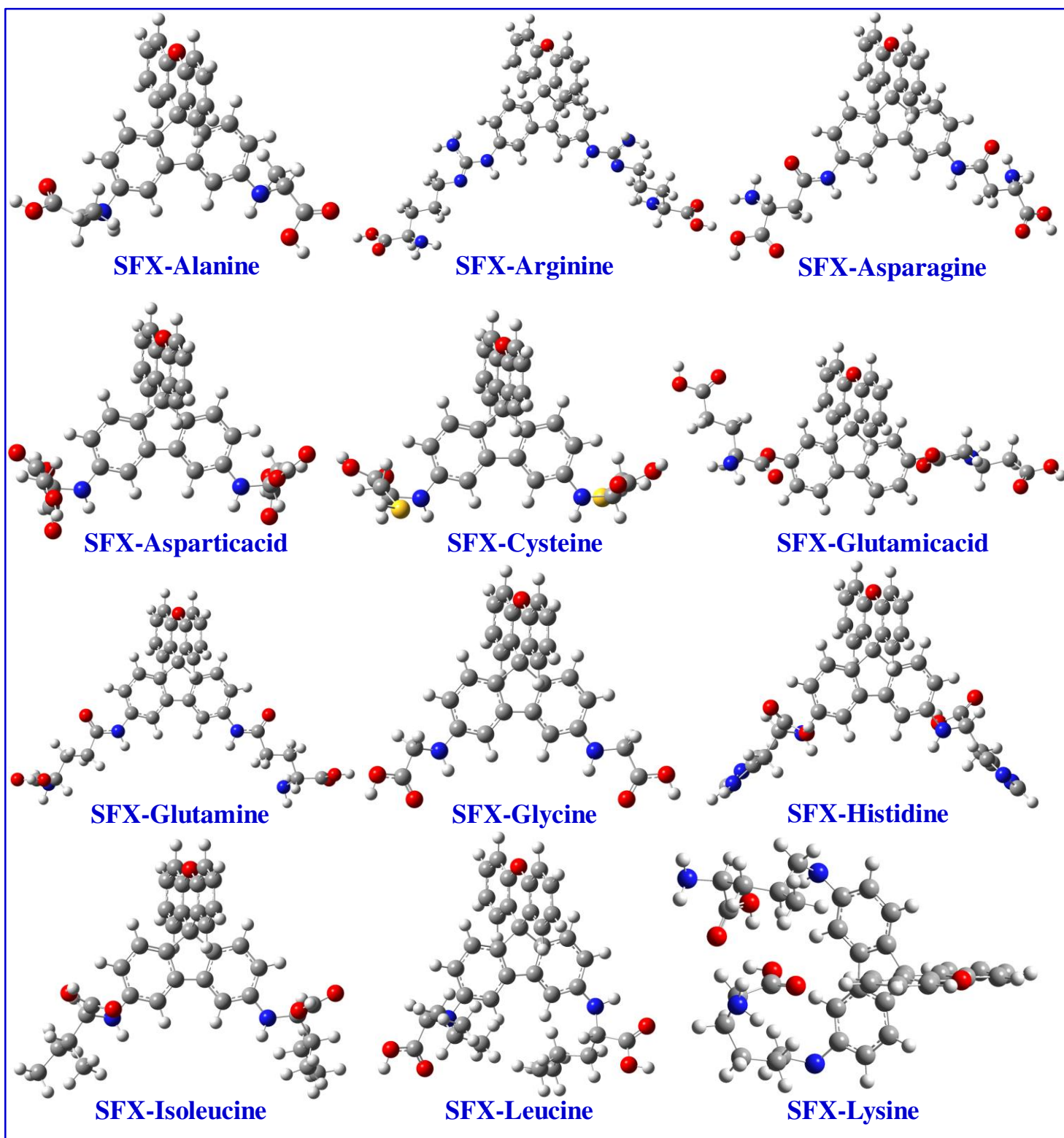
Fig. 2. Optimized geometries of designed molecules.

SFX-Methionine

SFX-Phenylalanine

SFX-Proline

SFX-Selenocysteine

SFX-Serine

SFX-Threonine

SFX-Tryptophan

SFX-Tyrosine

SFX-Valine
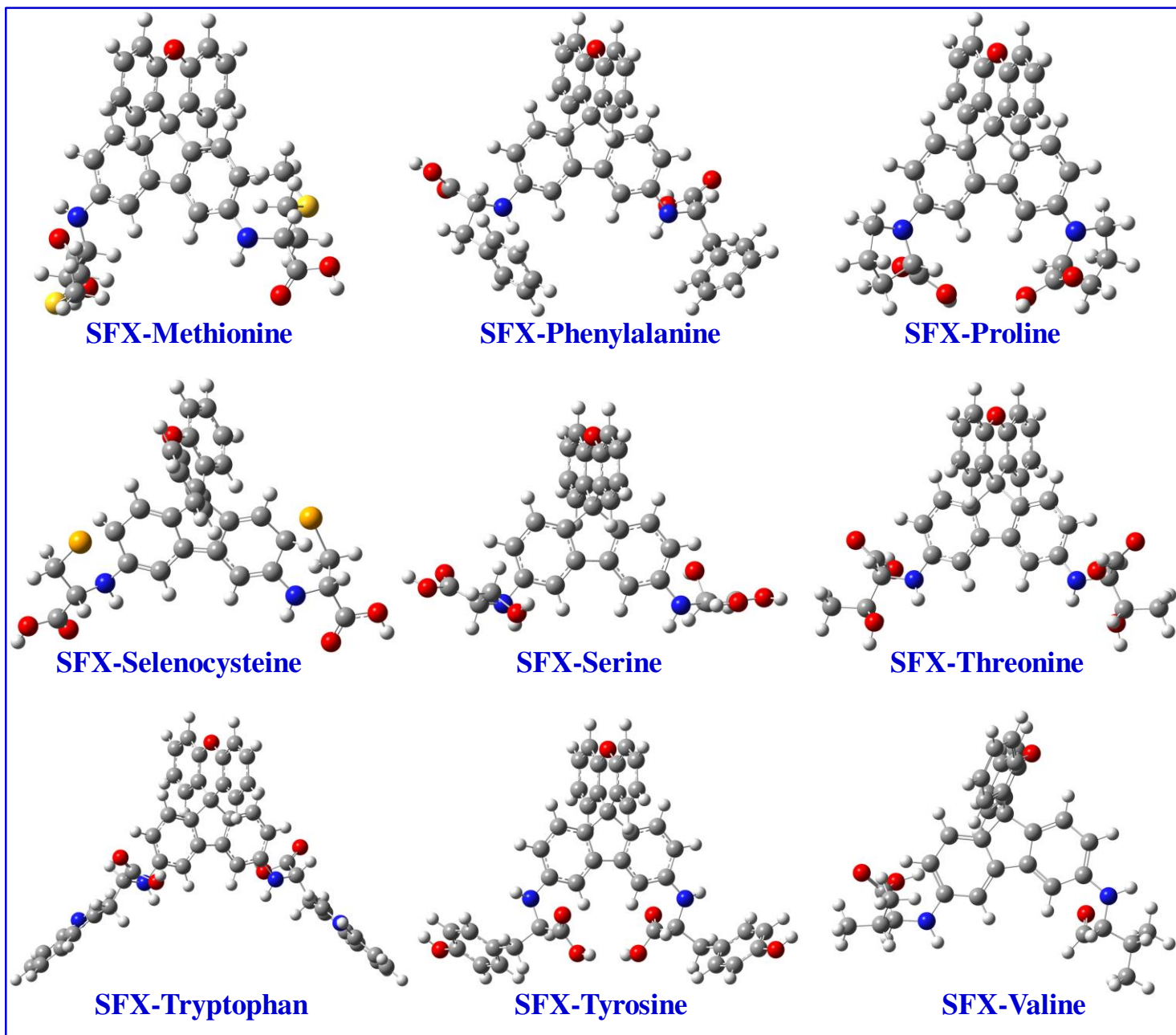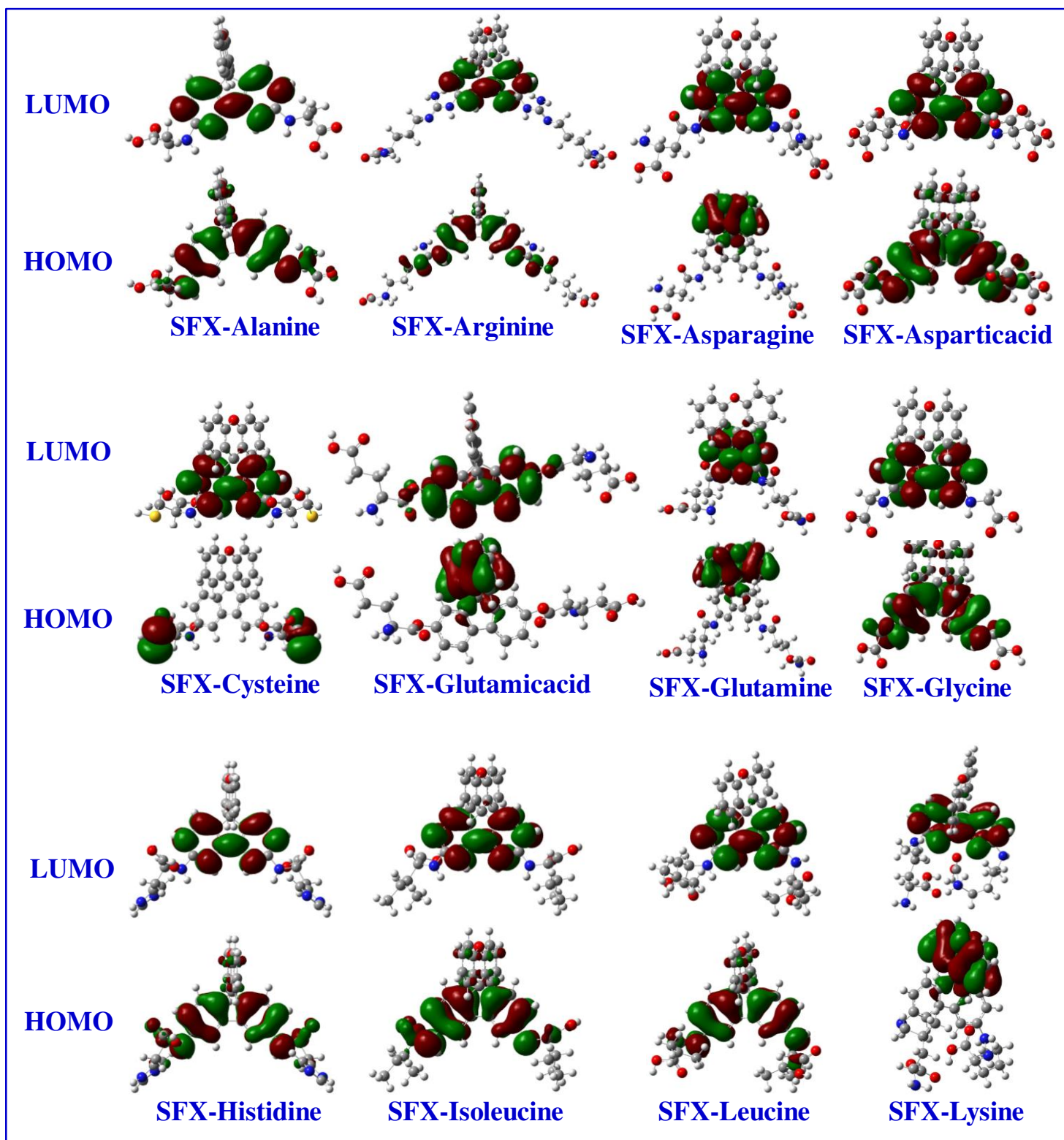
Fig. 2. Continued.

Fig. 3. HOMO and LUMO orbitals of designed HTM molecules.

LUMO

HOMO

SFX-Methionine

SFX-Phenylalanine

SFX-Proline

LUMO

HOMO

SFX-Selenocysteine

SFX-Serine

SFX-Threonine

LUMO

HOMO

SFX-Tryptophan

SFX-Tyrosine

SFX-Valine
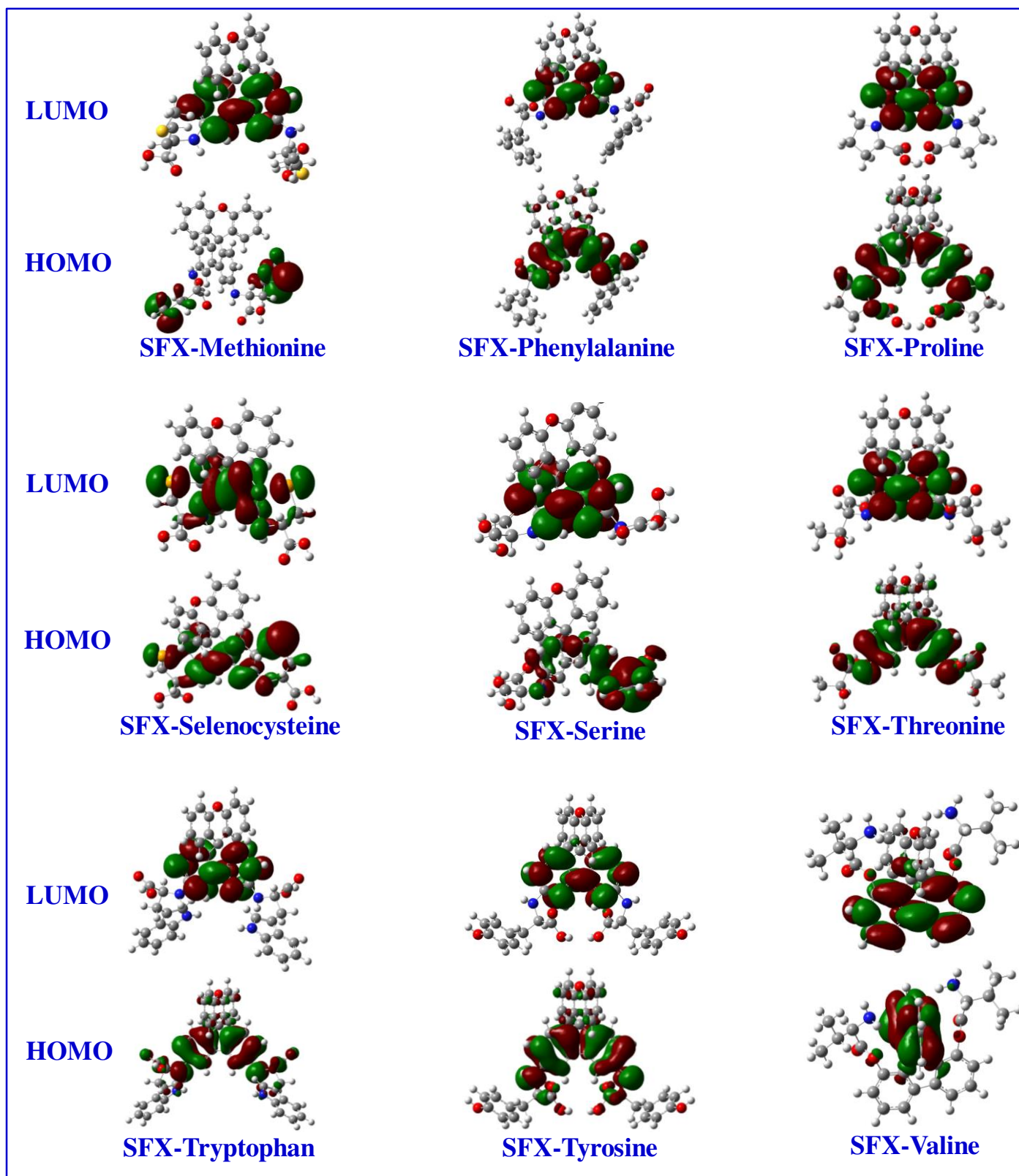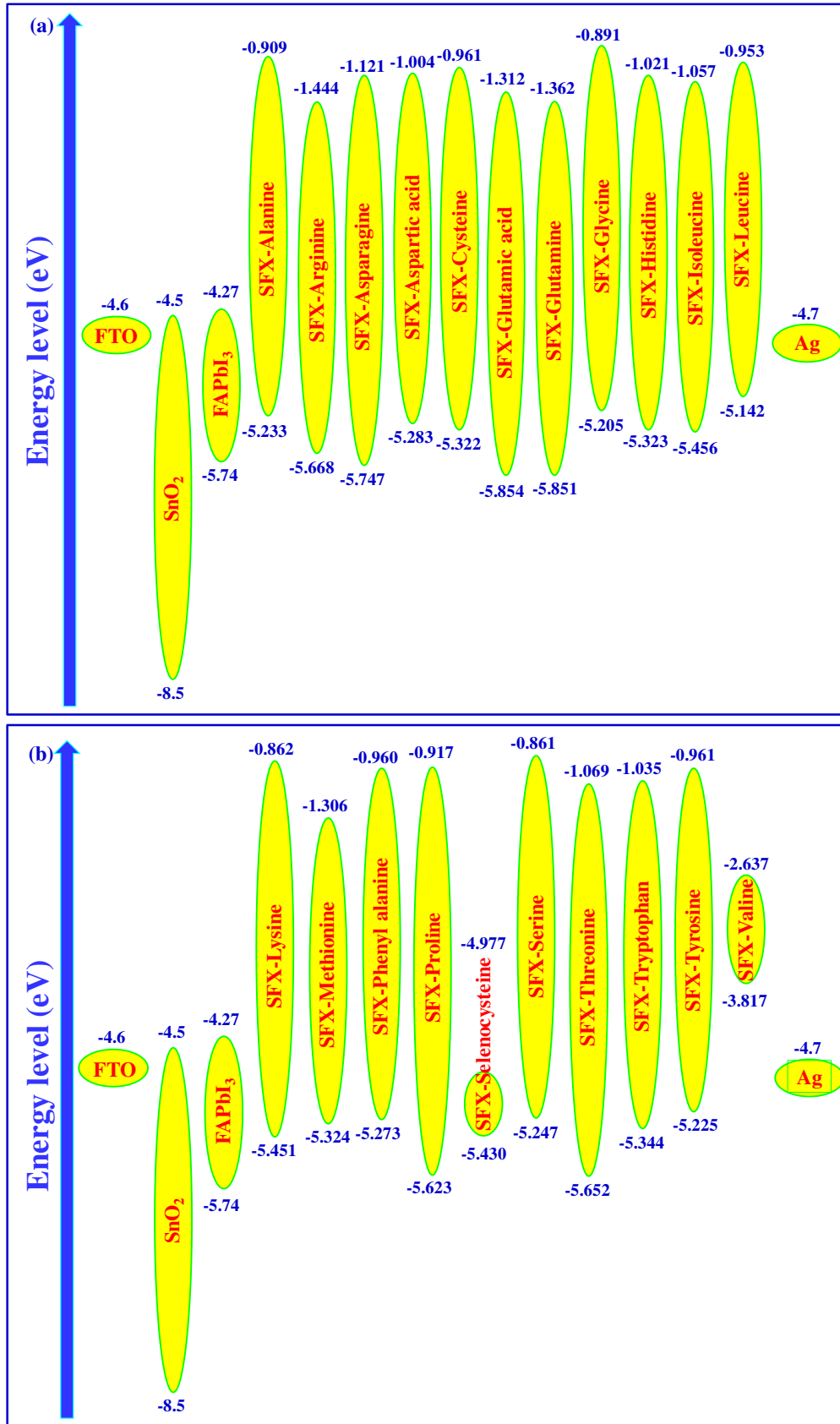
Fig. 3. Continued.

Fig. 4. Energy levels of FTO, SnO₂, perovskite FAPbI₃, SFX-based HTMs, and Ag cathode.
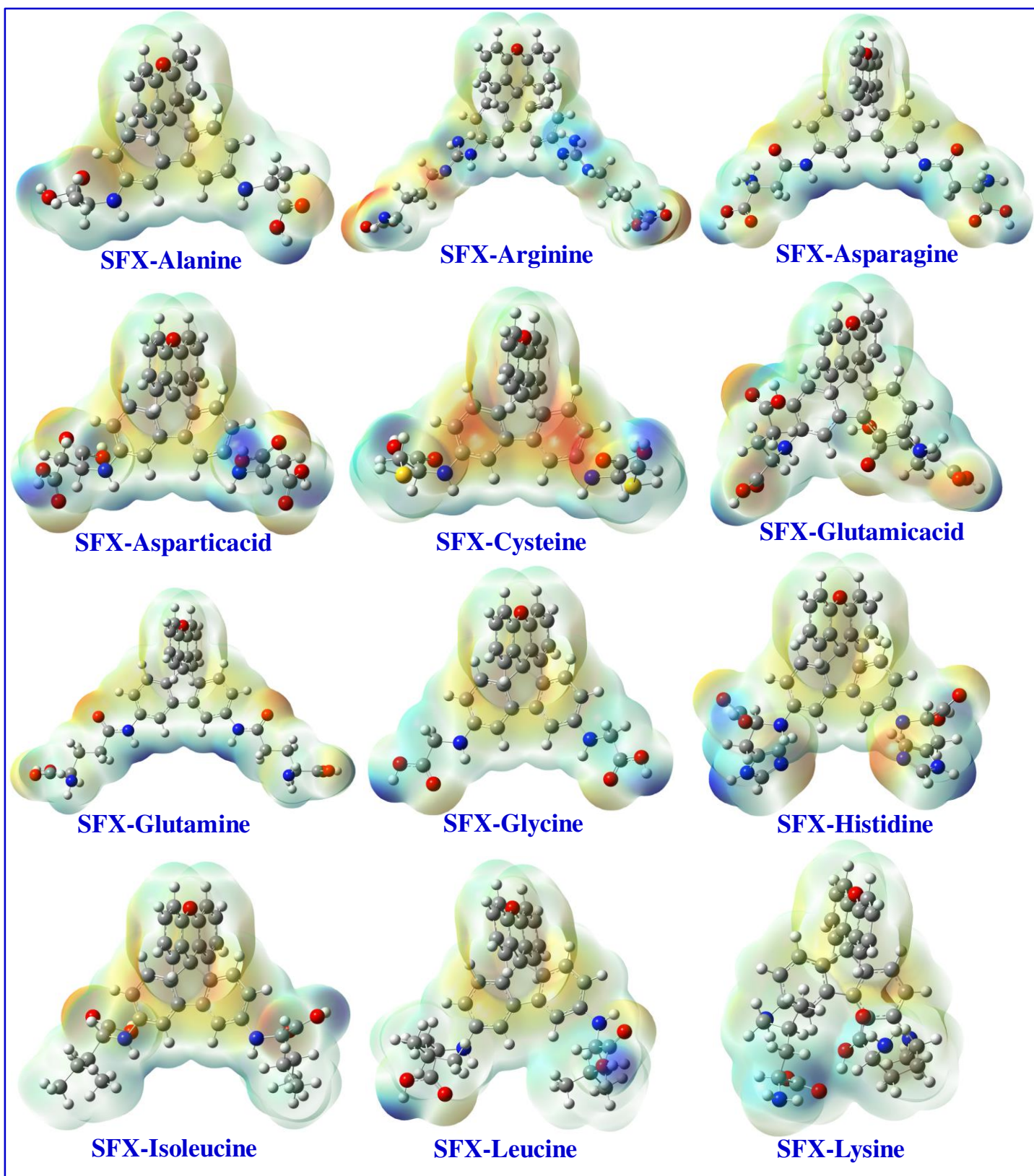
Fig. 5. ESP maps of all SFX-based HTM derivatives calculated in dichloromethane.

SFX-Methionine

SFX-Phenylalanine

SFX-Proline

SFX-Selenocysteine

SFX-Serine

SFX-Threonine

SFX-Tryptophan

SFX-Tyrosine

SFX-Valine
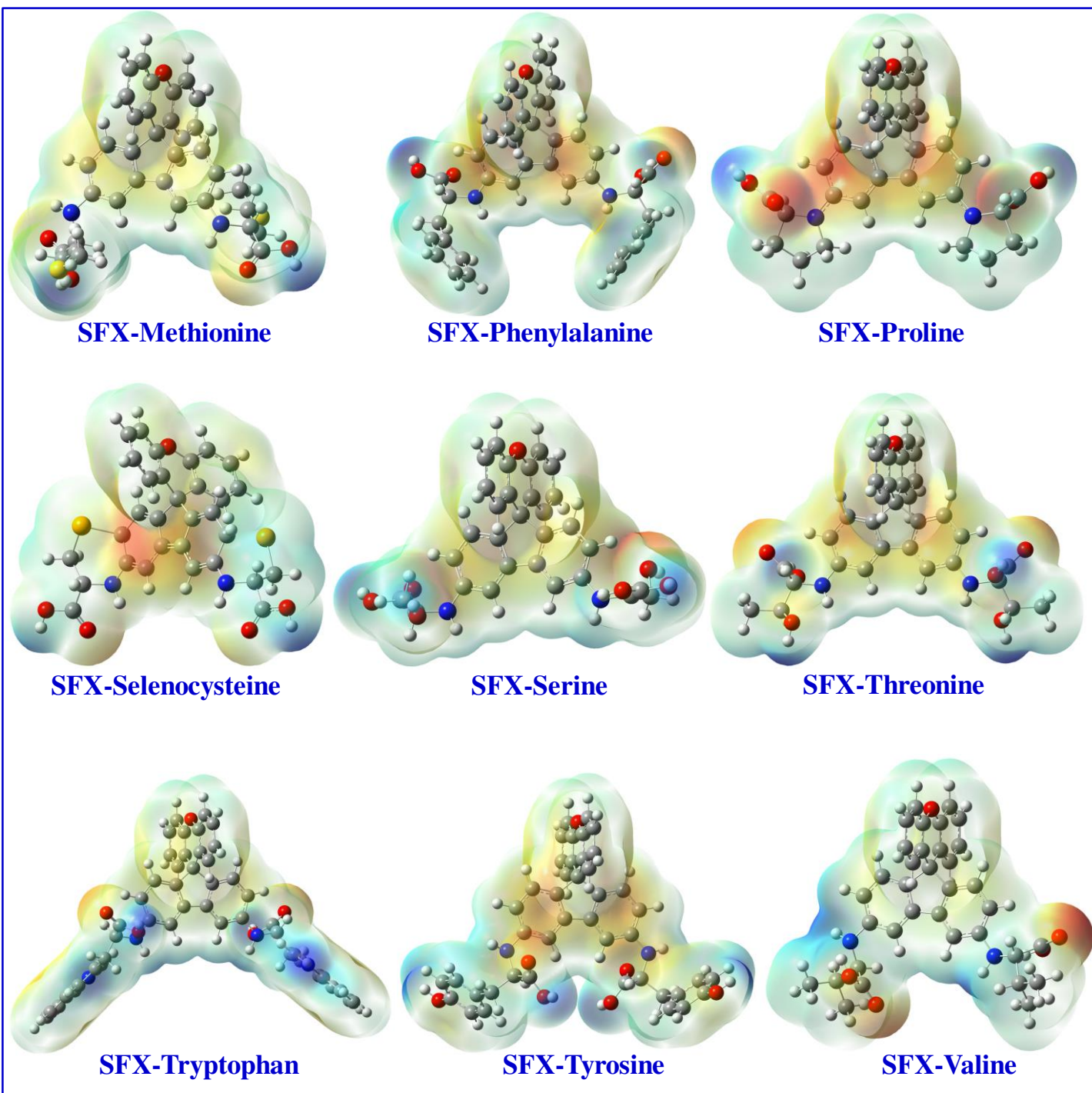
Fig. 5. Continued.
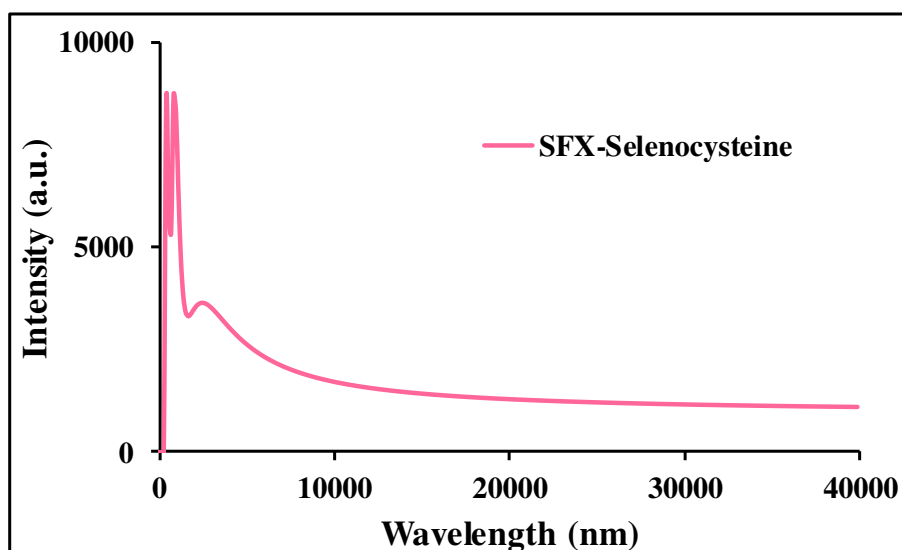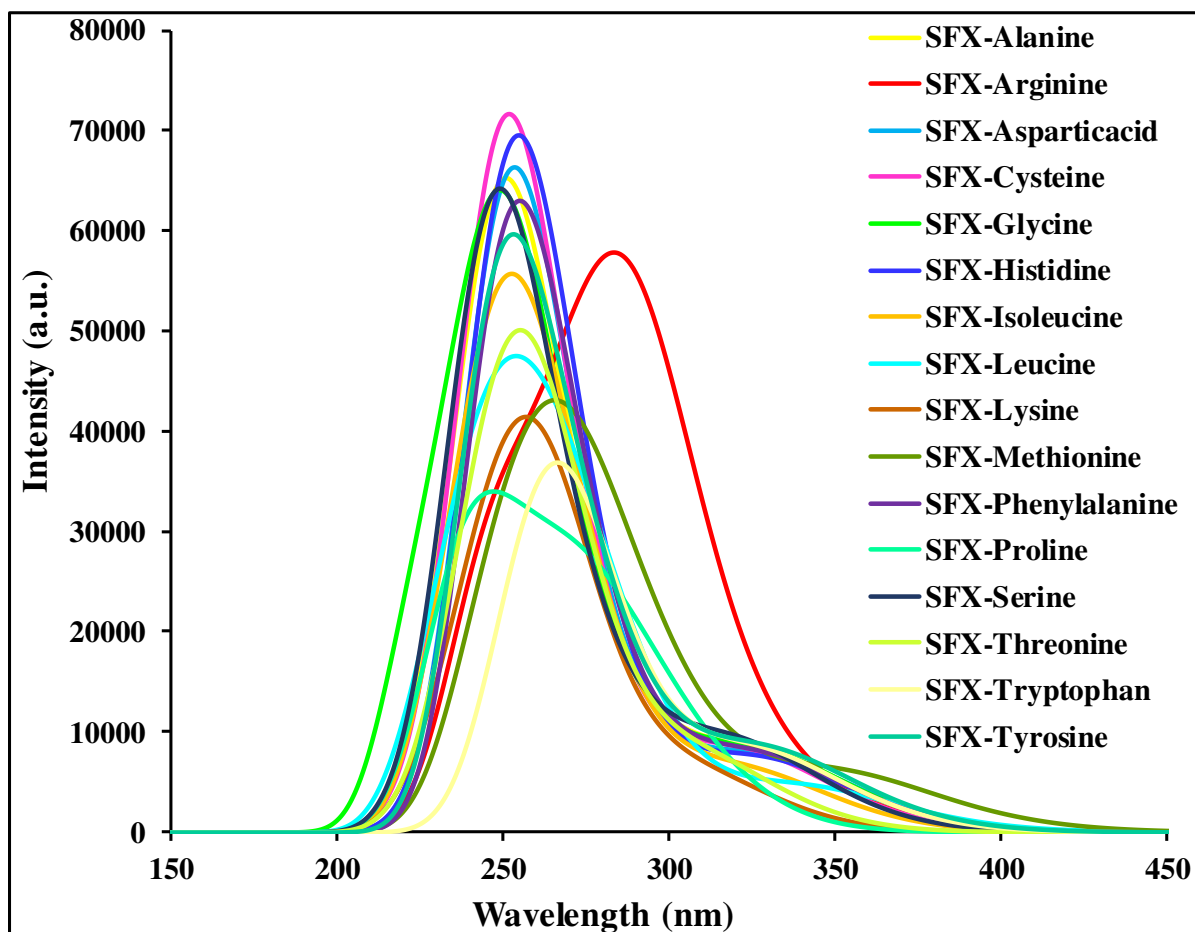
Fig. 6. Absorption spectra of HTM derivatives within CH_2Cl_2 solvent.
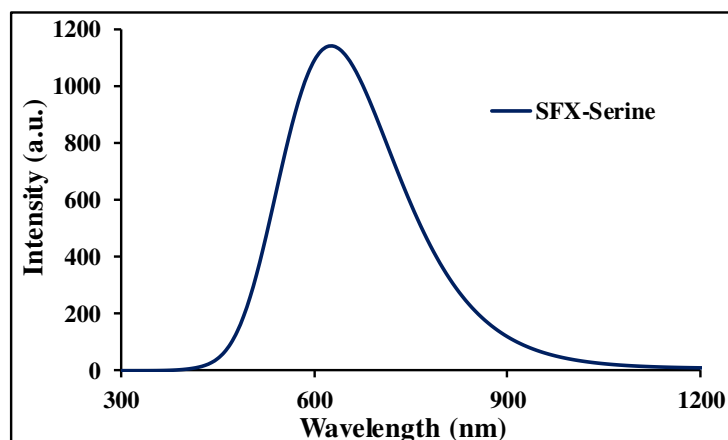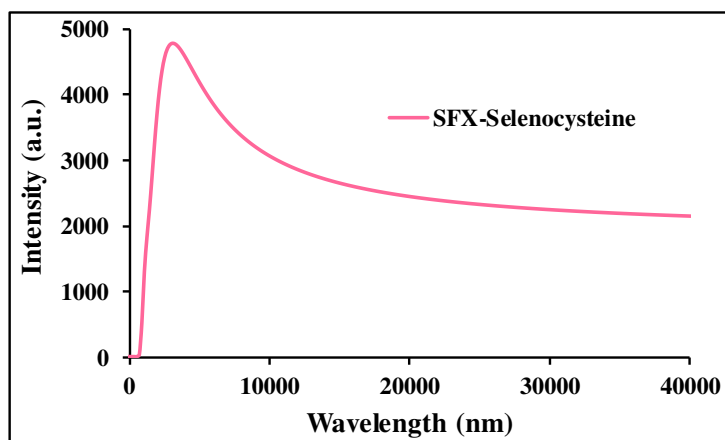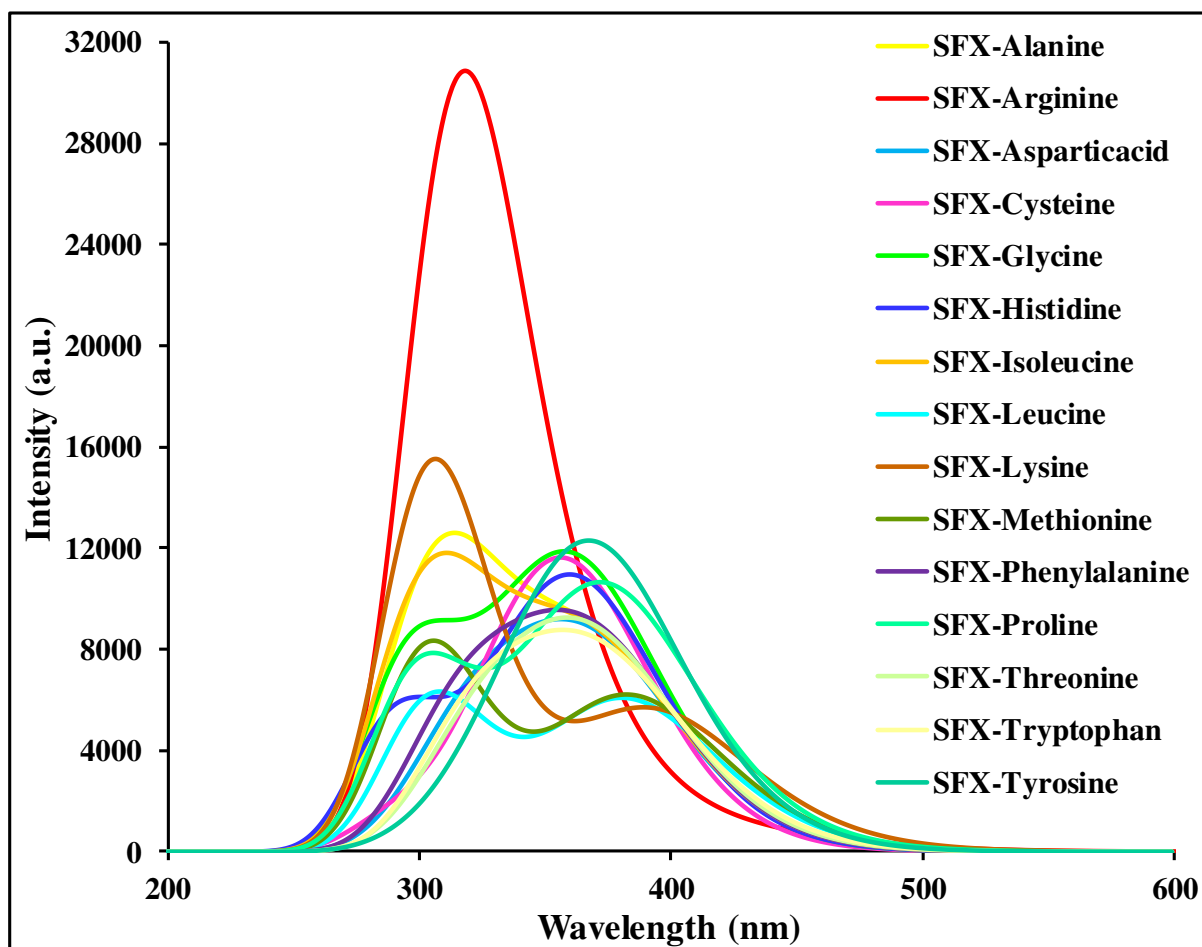
Fig. 7. Emission PL spectra of HTM derivatives calculated within CH$_2$Cl$_2$ solvent.
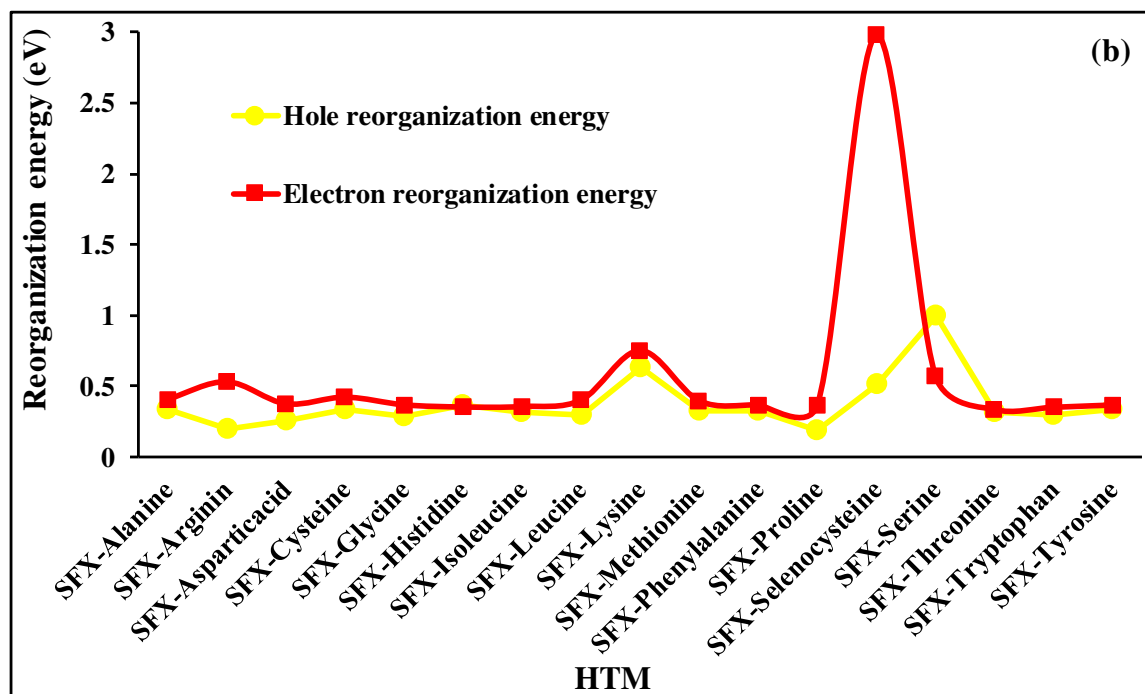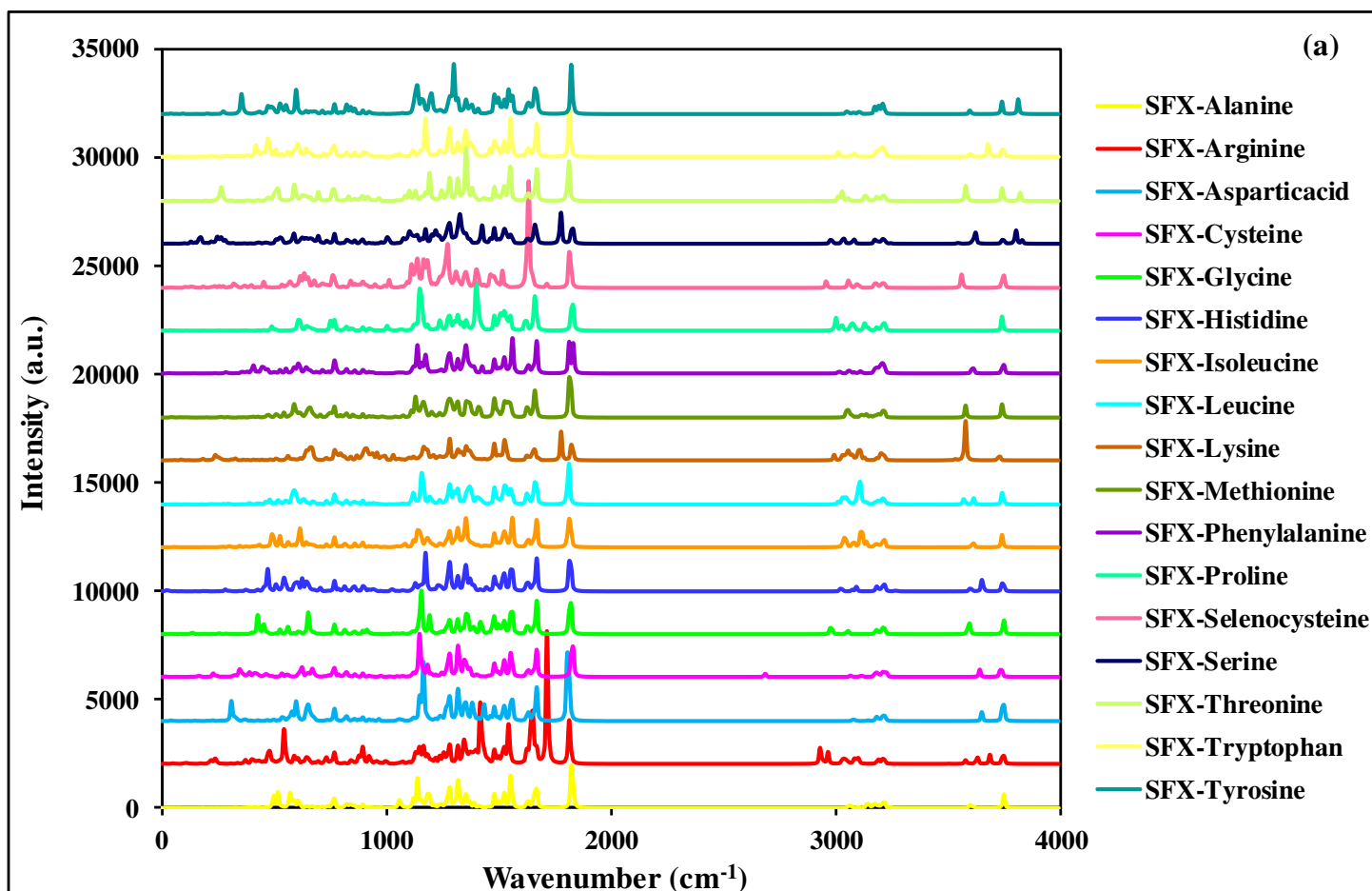
Fig. 8. (a) Infrared spectra of HTM samples calculated in dichloromethane solution. (b) Changes of electron and hole reorganization energies of HTMs.
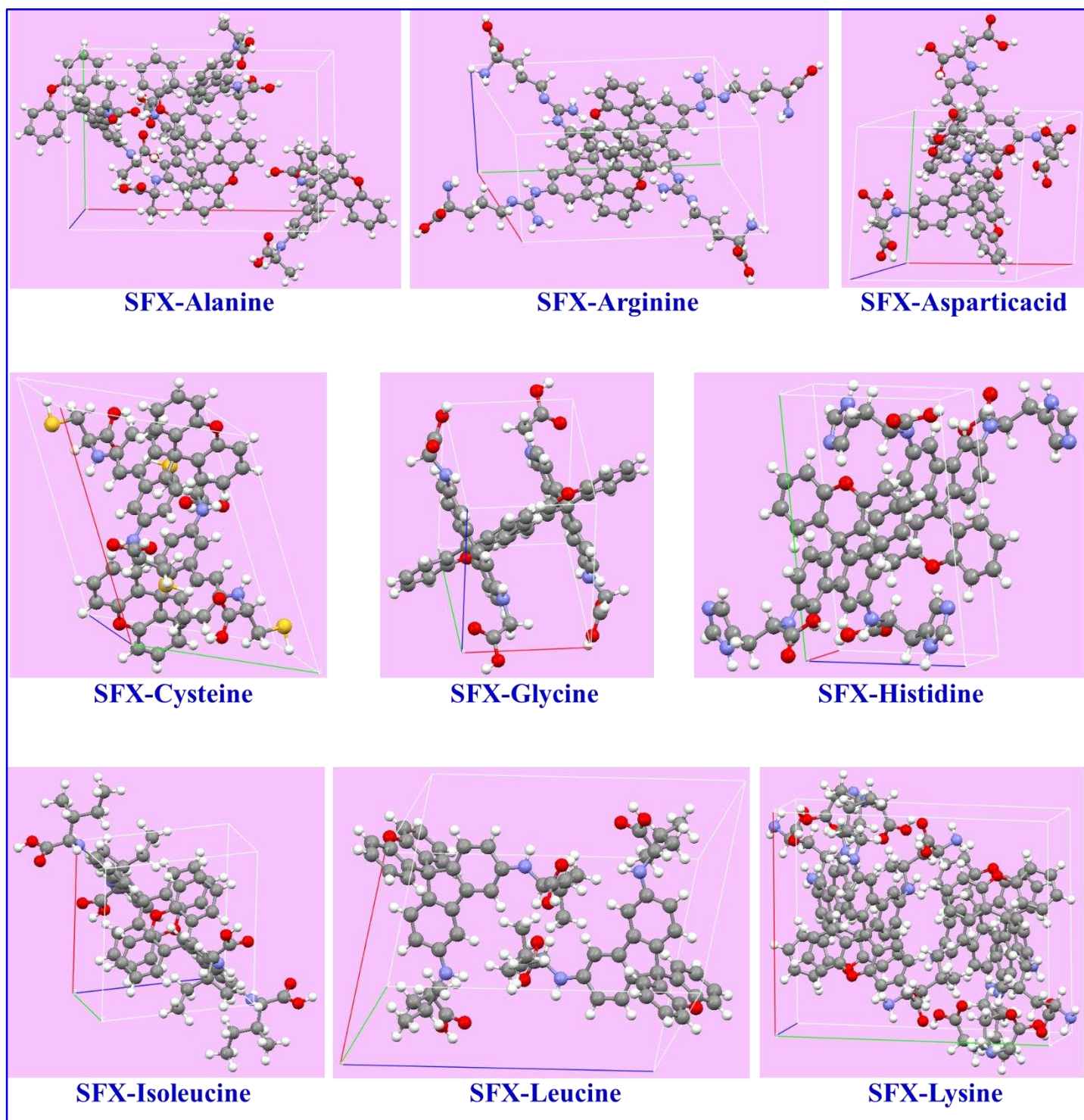
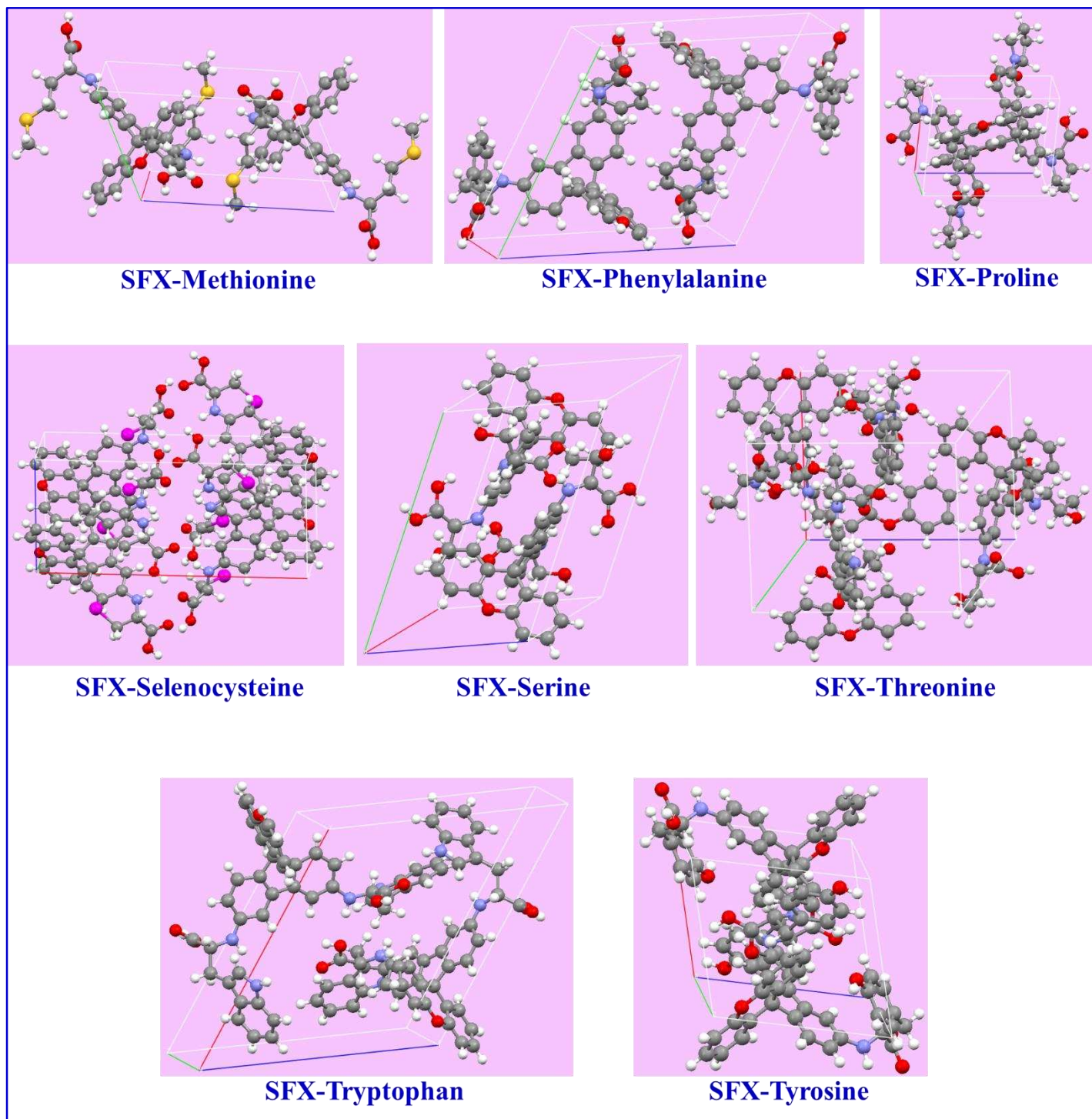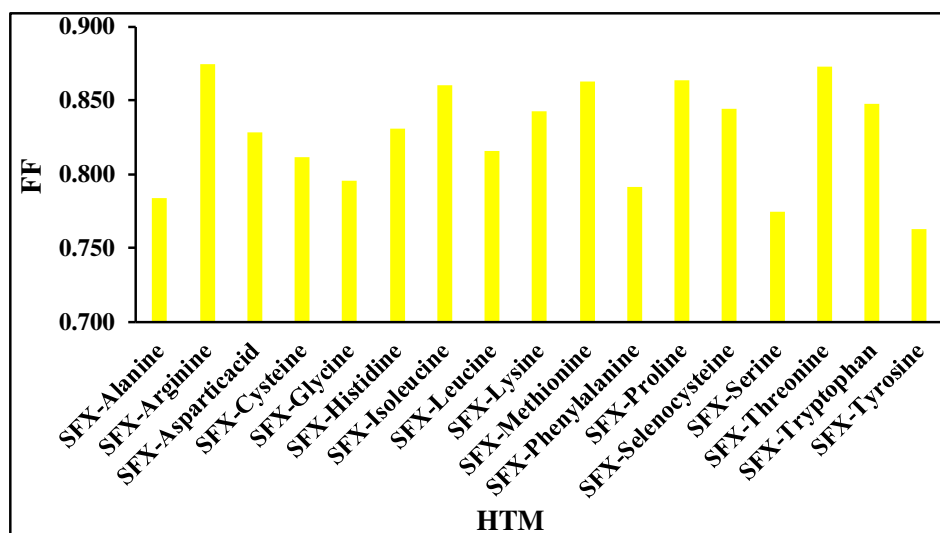**Fig. 9.** Unit cells of SFX-based HTM crystal structures with the highest stability.

SFX-Methionine

SFX-Phenylalanine

SFX-Proline

SFX-Selenocysteine

SFX-Serine

SFX-Threonine

SFX-Tryptophan
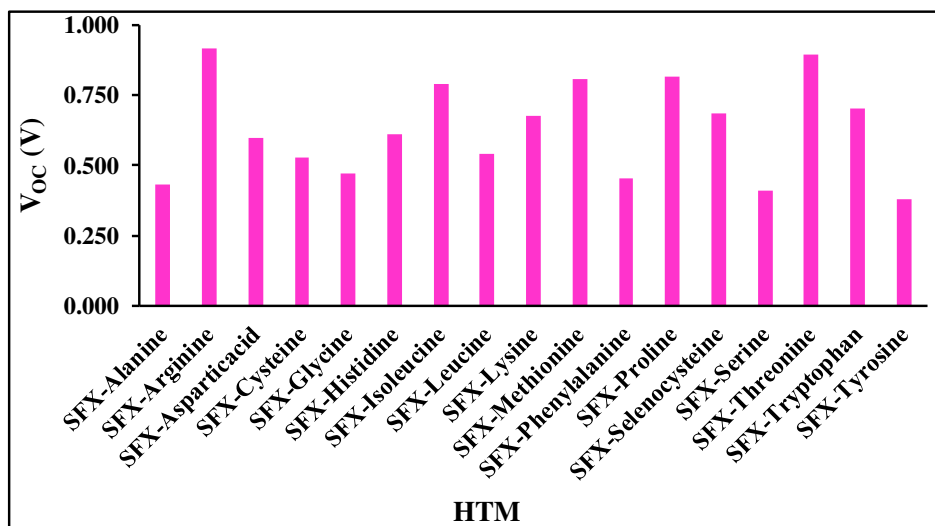
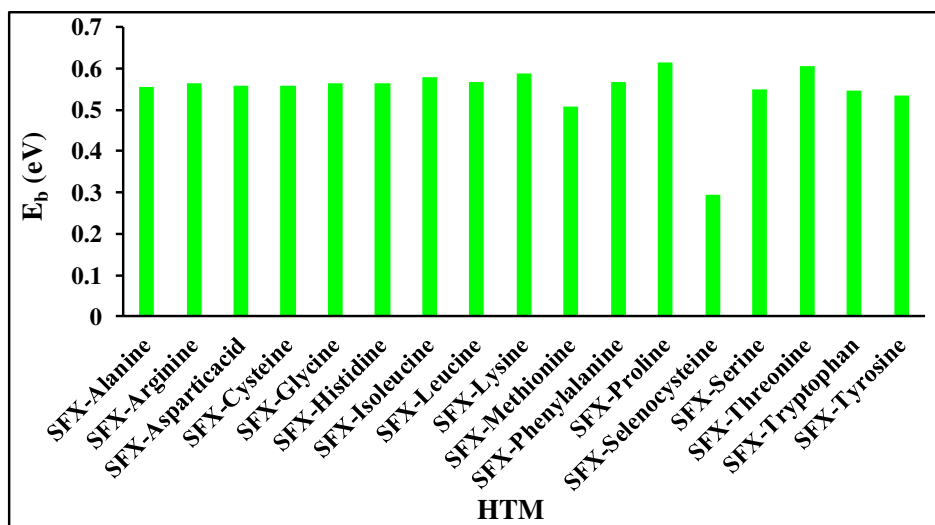**SFX-Tyrosine**

Fig. 9. Continued.

Fig. 10. Variations of E_b, V_{OC}, and FF values of HTM derivatives calculated in dichloromethane solution.